Facing diseases caused by trypanosomatid parasites: rational design of multifunctional oxidovanadium(IV) complexes with bioactive ligands

Gonzalo Scalese[1]*, Ignacio Machado[2], Fabiana Salazar[3], E. Laura Coitiño[3], Isabel Correia[4], João Costa Pessoa[4], Leticia Pérez-Díaz[5]* and Dinorah Gambino[1]*

[1]Área Química Inorgánica, Departamento Estrella Campos, Facultad de Química, Universidad de la República, Montevideo, Uruguay, [2]Área Química Analítica, Departamento Estrella Campos, Facultad de Química, Universidad de la República, Montevideo, Uruguay, [3]Laboratorio de Química Teórica y Computacional, Instituto de Química Biológica, Facultad de Ciencias y Centro de Investigaciones Biomédicas, Universidad de la República, Montevideo, Uruguay, [4]Centro de Química Estrutural, Institute of Molecular Sciences Departamento de Engenharia Química, Instituto Superior Técnico, Universidade de Lisboa, Lisboa, Portugal, [5]Sección Genómica Funcional, Instituto de Química Biológica, Facultad de Ciencias, Universidad de la República, Montevideo, Uruguay

Searching for new prospective drugs against Chagas disease (American trypanosomiasis) and Leishmaniasis, a series of five heteroleptic vanadium compounds, [V^{IV}O(L-H)(mpo)], where L are 8-hydroxyquinoline derivatives and mpo is 2-mercaptopyridine N-oxide, are synthesized and characterized. Comprehensive characterizations are conducted in solid state and in solution. The compounds are evaluated on epimastigotes and trypomastigotes of *Trypanosoma cruzi* and in promastigotes of *Leishmania infantum*, alongside on VERO cells, as a mammalian cell model. The compounds exhibit activity against both forms of *T. cruzi* and promastigotes of *L. infantum*, with the trypomastigote infective stage of *T. cruzi* displaying the highest sensitivity. The most selective vanadium compound [V^{IV}O(L2-H)(mpo)], with L2 = 5-chloro-7-iodo-8-hydroxyquinoline, globally shows adequate selectivity towards the parasite and was selected to carry out further in-depth biological studies. [V^{IV}O(L2-H)(mpo)] significantly impacted the infection potential of cell-derived trypomastigotes and hindered the replication of the *T. cruzi* amastigote form. Low total vanadium uptake by *T. cruzi* parasites and preferential accumulation in the soluble proteins fraction, with negligible localization in the DNA fraction, are determined. A trypanocide effect is observed across various concentrations of the compound. The generation of oxidative stress and the induction of mitochondria-dependent apoptosis are proposed as the main mechanisms of the parasite's death by the V^{IV}O compounds. Both theoretical predictions and experimental data support the hypothesis that inhibiting the parasite-specific enzyme NADH-fumarate reductase activity plays a crucial role in the trypanocidal action of these complexes. Globally, [V^{IV}O(L-H)(mpo)] complexes could be considered interesting anti-*T. cruzi* agents that deserve further research.

KEYWORDS

vanadium-based drugs, 8-hydroxyquinolines, multifunctional complexes, *Trypanosoma cruzi*, *Leishmania*

1 Introduction

Chagas disease, also known as American trypanosomiasis, and Leishmaniasis are infectious diseases caused by closely related trypanosomatid protozoan parasites. These maladies cast a long shadow over underprivileged regions within developing countries and coexist as co-endemic in South America. They are classified by the World Health Organization as neglected tropical diseases, primarily due to the pharmaceutical industry's lack of interest in drug development (De Rycker et al., 2018; Santos et al., 2020; Kourbeli et al., 2021; World Health Organization, 2023c). Chagas disease is caused by the protozoan parasite *Trypanosoma cruzi* (*T. cruzi*) and currently affects about 6–7 million people. The disease can lead to severe cardiac and gastrointestinal complications if left untreated and is mainly transmitted to the mammalian hosts by the bite of infected blood-sucking bugs. Due to the migration of people bearing the disease in the silent indeterminate phase, this parasitosis has expanded to non-endemic regions of the world, namely, some countries in North America, Europe, Asia, and Oceania. These migrants transmit the disease through organ transplantation, blood transfusion, and from mother to fetus (De Rycker et al., 2018; Santos et al., 2020; Kourbeli et al., 2021; World Health Organization, 2023c; World Health Organization, 2023a). Leishmaniasis is caused by no fewer than 20 discrete *Leishmania* species that affect about 350 million people, widespread in 98 countries of four continents. The pathogen is mainly transmitted to mammals by the bite of female-infected sandflies. The disease shows three forms with different levels of severity, namely, visceral leishmaniasis, cutaneous leishmaniasis, and mucocutaneous leishmaniasis. Visceral leishmaniasis is fatal if left untreated (Nagle et al., 2014; Burza et al., 2018; Kwofie et al., 2020; Brindha et al., 2021; Kourbeli et al., 2021; World Health Organization, 2023b).

The current chemotherapy for treating these diseases is decades old and shows important therapeutic disadvantages, such as several toxic side effects, development of resistance, and need for long treatments. Consequently, there is an urgent need to develop more efficient and safe new drugs (Nagle et al., 2014; Santos et al., 2020; Brindha et al., 2021; Kourbeli et al., 2021).

The rational design of metal-based drugs, either coordination or organometallic compounds, has been demonstrated to be a suitable strategy for developing new prospective agents against *T. cruzi* and *Leishmania spp* (Sánchez-Delgado and Anzellotti, 2004; Sánchez-Delgado et al., 2004; Navarro, 2009; Navarro et al., 2010; Gambino, 2011; Gambino and Otero, 2012; Tahghighi, 2014; Brown and Hyland, 2015; Pessoa et al., 2015; Gambino and Otero, 2018; Zhang et al., 2018; Gambino et al., 2019; Ong et al., 2019; Minori et al., 2020; Gambino and Otero, 2021; Navarro et al., 2021; Gambino et al., 2023). Our group's recent efforts have focused on the rational design of multifunctional metal compounds by hybridization of different pharmacophoric scaffolds (Rivas et al., 2021; Soba et al., 2023). This strategy could lead to multi-target compounds showing dual or even multiple modes of action (Viegas-Junior et al., 2007; Gibson, 2019; Kenny and Marmion, 2019). These hybrids include in a single molecule a pharmacologically relevant metal center, one or more bioactive ligands that show *per se* the desired biological activity, and suitable co-ligands that show antiparasitic activity and/or modulate physicochemical properties

of biological importance, like water solubility or lipophilicity (Gambino et al., 2019; Gambino and Otero, 2021; Gambino et al., 2023). As part of this research, we have developed many vanadium-based compounds that showed interesting biological properties against the parasites (Gambino, 2011; Pessoa et al., 2015; Scalese et al., 2015; Scalese et al., 2017a; Scalese et al., 2017b; Scalese et al., 2018; Scalese et al., 2019; Scalese et al., 2021).

In the current work, we expanded our research on vanadium-based antiparasitic prospective drugs through the development of five novel oxidovanadium(IV) heteroleptic compounds, [V^{IV}O(L-H)(mpo)]. The new compounds include two different bidentate bioactive ligands: an 8-hydroxyquinoline (8HQ) derivative (L0-L4) and 2-mercaptopyridine *N*-oxide (mpo) (Figure 1A). The 8-hydroxyquinoline scaffold has been considered a privileged structure in drug discovery due to the significant biological activities observed for derivatives of this molecular framework (Song et al., 2015; Oliveri and Vecchio, 2016; Gupta et al., 2021; Joaquim et al., 2021).

The selected L0-L4 derivatives have previously demonstrated activity against non-infective epimastigote and infective trypomastigote forms of *T. cruzi*, and against the promastigote form of *L. infantum* (Scalese et al., 2019; Scalese et al., 2021; Rivas et al., 2022). High potency against all stages of *T. cruzi* and low unspecific toxicity on mammalian cells was previously reported for free mpo. Its main molecular target is the NADH-dependent fumarate reductase enzyme (*Tc*FR). This enzyme catalyzes the conversion of fumarate to succinate, which is one of the primary respiratory substrates of the parasite and is, therefore, required for energy production. In addition, the enzyme is present in the different life cycle stages of *T. cruzi* and *Leishmania* and is absent in the mammalian host, providing a suitable target for drug discovery (Turrens et al., 1999; Tobin et al., 2002). Accordingly, our group has reported several compounds bearing mpo as a ligand and selected metal centers that showed promising anti-*T. cruzi* activity and biological properties (Vieites et al., 2008; Vieites et al., 2009; Machado et al., 2014).

The five novel Oxidovanadium(IV) heteroleptic compounds here reported, [V^{IV}O(L-H)(mpo)] with L=L0-L4 (Figure 1B), were synthesized and fully characterized in solid state and solution using different independent techniques. The compounds were evaluated on epimastigotes and trypomastigotes of *T. cruzi*, promastigotes of *L. infantum*, and on VERO cells as mammalian cell model. Inhibition of *T. cruzi* fumarate reductase was experimentally and theoretically studied, searching for a correlation with biological activity. Additionally, the generation of ROS and the integrity of mitochondrial membrane potential in the parasite by effect of the compounds is investigated. Metallomics evaluation (uptake by the parasite and association to biomolecules) is also reported together with a series of relevant biological effects in *T. cruzi*. Once the biological action of the complexes takes place with the use of μM concentrations, relevance is also given to the probable hydrolysis of the reported vanadium complexes in biological media. In this context, as in other systems, the prepared compounds probably act as pro-drugs (Levina et al., 2017; Levina and Lay, 2017; Nunes et al., 2020; Santoro et al., 2020; Nunes et al., 2021). The whole set of results emerging from this work validates our design strategy and demonstrates the potentiality of new multifunctional oxidovanadium(IV) compounds as promising candidates for further development of vanadium agents against trypanosomatid parasites.

FIGURE 1
Structural formulae of: **(A)** the selected 8-hydroxyquinoline derivatives L0−L4 and the mpo ligand. **(B)** The new [V^{IV}O(L-H)(mpo)] complexes.
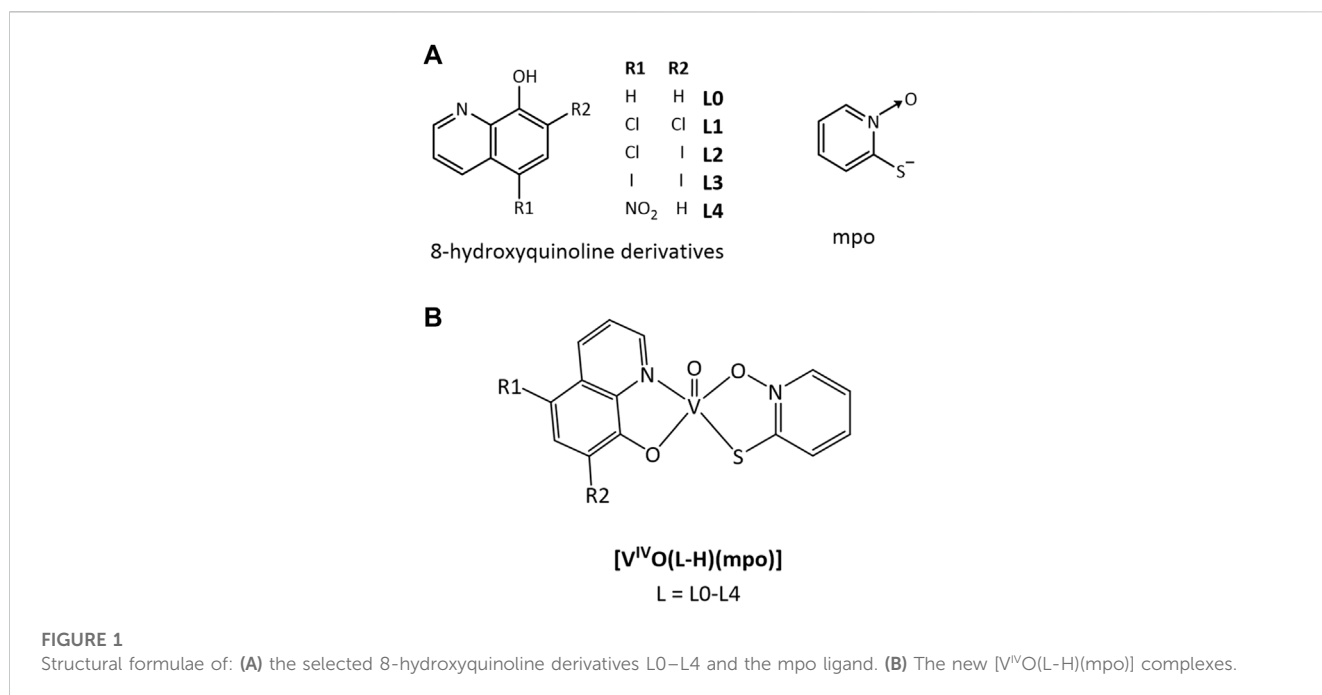
2 Materials and methods

2.1 Chemical reagents

All the chemical reagents were acquired from commercial sources and used without further purification. 8-hydroxyquinoline derivatives, 2-mercaptopyridine N-oxide sodium salt (Na mpo), and vanadium precursors were obtained from Sigma-Aldrich.

2.2 Synthesis of the heteroleptic oxidovanadium(IV) complexes [V^{IV}O(L−H)(mpo)], L = L0-L4

The novel [V^{IV}O(L-H)(mpo)] complexes, where L = L0 - L4 (Figure 1B), were synthesized according to the following procedure. Working under inert atmosphere, 0.5 mmol of L (73 mg of L0; 107 mg of L1; 153 mg of L2; 199 mg of L3; 95 mg of L4) and 0.5 mmol of Na mpo were dissolved in 6 mL of a 0.2 M NaOH aqueous solution. 0.5 mmol of V^{IV}OSO$_4$·5H$_2$O dissolved in 3 mL of water were added to the previous brown-greenish solution. Immediately, a brown solid appeared in suspension; it was stirred at room temperature for an hour. The solid was separated, washed with 5 portions of 2 mL water, 2 portions of 3 mL EtOH, and dried under vacuum for a week.

[V^{IV}O(L0-H)(mpo)]·1.5H$_2$O. Yield: 31 mg, 17%. Anal. (%) calc. for C$_{14}$H$_{13}$N$_2$O$_{4.5}$SV: C, 46.10; H, 3.61; N, 7.75; Found: C, 45.86; H, 3.45; N, 7.73. FTIR (KBr/cm^{-1}): 1188 ν(N-O), 830 δ (N-O), 697 ν(C-S), 968 ν(V=O).

[V^{IV}O(L1-H)(mpo)]·H$_2$O. Yield: 80 mg, 38%. Anal. (%) calc. for C$_{14}$H$_{10}$Cl$_2$N$_2$O$_4$SV: C, 39.62; H, 2.40; N, 6.61; Found: C, 39.51; H, 2.24; N, 6.78. FTIR (KBr/cm^{-1}): 1188 ν(N-O), 830 δ (N-O), 697 ν(C-S), 968 ν(V=O).

[V^{IV}O(L2-H)(mpo)]·3H$_2$O. Yield: 103 mg, 37%. Anal. (%) calc. for C$_{14}$H$_{14}$ClIN$_2$O$_6$SV: C, 30.54; H, 2.43; N, 5.12; Found: C, 30.48; H, 2.20; N, 5.03. FTIR (KBr/cm^{-1}): 1188 ν(N-O), 829 δ (N-O), 695 ν(C-S), 968 ν(V=O).

[V^{IV}O(L3-H)(mpo)]. Yield: 87 mg, 30%. Anal. (%) calc. for C$_{14}$H$_8$I$_2$N$_2$O$_3$SV: C, 28.67; H, 1.40; N, 4.83; Found: C, 29.20; H, 1.64; N, 5.01. FTIR (KBr/cm^{-1}): 1188 ν(N-O), 829 δ (N-O), 696 ν(C-S), 967 ν(V=O).

[V^{IV}O(L4-H)(mpo)]·H$_2$O. Yield: 70 mg, 35%. Anal. (%) calc. for C$_{14}$H$_{11}$N$_3$O$_6$SV: C, 42.04; H, 2.80; N, 10.52; Found: C, 42.12; H, 2.51; N, 10.50. FTIR (KBr/cm^{-1}): 1188 ν(N-O), 830 δ (N-O), 696 ν(C-S), 966 ν(V=O).

2.3 Physicochemical characterization

2.3.1 Characterization in solid state

C, N and H analyses were conducted using a Thermo Scientific Flash 2000 elemental analyzer with an Eager 200 data processor. Thermogravimetric analyses (TGA) were carried out using a Shimadzu TGA 50 thermal balance with a platinum cell. The analysis was conducted under air flow (50 mL/min) and with a heating rate of 0.5°C/min (from room temperature to 80°C), 1.0°C/min (from 80°C to 400°C), and 30°C/min (from 400°C to 700°C). The FTIR spectra (4,000–400 cm^{-1}) were recorded in a Shimadzu IRPrestige-21 instrument on KBr pellets.

2.3.2 Characterization in solution

Conductivity experiments were performed at 25°C in 1 mM dimethyl sulfoxide (DMSO) solutions using a CON 700 OAKTON conductivity meter. Electronic paramagnetic resonance (EPR) spectra were acquired at 100 K using a Bruker 300E X-band spectrometer coupled with a Bruker ER041 X-band frequency counter (9.45 GHz). The compounds were dissolved at

concentrations of 3 mM in DMSO, which was previously degassed by bubbling with N_2 for 10 min at room temperature, and the spectra were measured immediately. Spin Hamiltonian parameters were obtained through simulation using the program developed by Rockenbauer and Korecz (Rockenbauer and Korecz, 1996). To assess the stability of the solution, they were left exposed to air for 21 h, and after that time, 5% D_2O was added. The EPR spectrum was re-measured, and concurrently, ^{51}V NMR spectra were recorded in a Bruker Avance III 400 MHz to detect changes in the oxidation state of the central atom. The ^{51}V NMR chemical shift values were referenced to V^VOCl_3 as an external standard. The electronic spectra of 3 mM DMSO solutions were measured at time 0 and 21 h, as well as in 0.3 mM concentration at time 0, using a Shimadzu UV-Vis 1900 spectrophotometer.

2.4 Biological studies

2.4.1 Cell culture and solutions
2.4.1.1 VERO cells
VERO cells (ATCC CCL81) were used as a mammalian model to assess nonspecific cytotoxicity and to establish *T. cruzi* infections. The cells were cultured at 37°C in RPMI-1640 medium supplemented with 10% of heat-inactivated fetal bovine serum (FBS) and 1% streptomycin (100 µg mL^{-1}), penicillin (10 µg mL^{-1}), in a humidified incubator with 5% CO_2. Every 72 h, the cells were washed with PBS, incubated for 3 min with 0.05% Trypsin-EDTA and subcultured (Ammerman et al., 2008).

2.4.1.2 *Trypanosoma cruzi*
All experiments involving *T. cruzi* were conducted using the CL Brener strain. Epimastigotes were maintained at 28°C in BHI-Tryptose medium supplemented with 10% heat-inactivated FBS and 1% streptomycin (100 µg mL^{-1}), penicillin (10 µg mL^{-1}). Cultures were subcultured every 72 h to maintain them in the exponential growth phase.

Nutritionally stressed epimastigotes (approximately 10 days without renewing the culture medium) were used to infect a monolayer of VERO cells at a ratio of 100:1 (parasites:cells) and incubated in the same conditions as those mentioned for VERO cells. After 24 h, parasites that remained outside the cells were removed by aspirating the culture medium. The infected cell monolayer was washed three times with 1× PBS and RPMI-1640 medium was added. The intracellular trypomastigotes that emerged from the VERO cells (4–5 days) were used to infect a new cell monolayer (MacLean et al., 2018). For activity assays, the intracellular trypomastigotes were obtained from the supernatant of infected VERO cells 72 h after establishing the infection.

2.4.1.3 *Leishmania infantum*
Promastigotes from the MHOM MA67I7MAP263 strain were cultured at 28°C in RPMI medium supplemented with 10% heat-inactivated fetal bovine serum (FBS) and 1% streptomycin (100 µg mL^{-1}), penicillin (10 µg mL^{-1}). Successive passages were performed every 72 h to maintain the parasites in the exponential growth phase.

2.4.1.4 Compounds' solutions
The compounds to be evaluated *in vitro* were dissolved in cell culture grade DMSO at stock concentration of 11.25 mM. The stock solutions were further diluted in a supplemented culture medium (BHI-Tryptose or RPMI-1640, as appropriate) to achieve the working concentrations. For each assessment, stock solutions were prepared immediately prior to dilution. The final concentration of DMSO in the culture medium did not exceed 1% v/v. This concentration of DMSO does not influence the cellular growth of *T. cruzi*, *L. infantum*, and VERO cells (Vieites et al., 2008).

2.4.2 *In vitro* activity against *Trypanosoma cruzi* and *Leishmania infantum*
2.4.2.1 Inhibition of *T. cruzi* epimastigotes and *L. infantum* promastigotes growth
The effect of the compounds on the proliferation was studied using the extracellular replicative forms of *T. cruzi* and *L. infantum* according to the previously reported procedure (Vieites et al., 2008; Benitez et al., 2009; Vieites et al., 2009; Benitez et al., 2011; Fernandez et al., 2013a; Fernandez et al., 2013b; Cipriani et al., 2014; Rodriguez Arce et al., 2015; Scalese et al., 2015; Scalese et al., 2017a; Scalese et al., 2017b; Mosquillo et al., 2018a; Mosquillo et al., 2018b; Scalese et al., 2018; Scalese et al., 2019; Mosquillo et al., 2020a; Mosquillo et al., 2020b; Rivas et al., 2022). Briefly, $1×10^6$ parasites/mL parasites were incubated for 5 days with at least 7 concentrations of the compounds in a 96-well culture plate. The percentage of cell growth was monitored by assessing the optical density of the culture at 595 nm (A) using a Thermo Scientific Varioskan Flash Multimode plate reader. The IC$_{50}$ for 5 days (the concentration causing 50% growth inhibition after 5 days of incubation) was determined by the formula: % parasite growth = $(A_p - A_{0p})/(A_c - A_{0c})$ x 100, where A_p is the A_{595} of the culture containing the compound on day 5, A_{0p} is the A_{595} of the culture containing the compound on day 0, A_c is the A_{595} of the culture in the absence of any drug (control) on day 5, and A_{0c} is the A_{595} in the absence of any drug on day 0. Dose-response curves were generated using GraphPad Prism version 8.00 for Windows. Experimental values were fitted to a sigmoidal curve, and IC$_{50}$ for 5 days values were interpolated from the equation. The results were presented as mean values ± standard deviation (SD) from three to six independent biological replicates. Nifurtimox or Amphotericin B served as the reference drugs for anti-*T. cruzi* or antileishmanial activity, respectively.

2.4.2.2 Viability of *T. cruzi* epimastigotes and trypomastigotes after 24 h of treatment
To evaluate the impact of the compounds after 24 h exposure on epimastigotes and trypomastigotes of *T. cruzi* (IC$_{50, \ 24 \ h}$), the resazurin reduction technique was utilized (Scalese et al., 2021). Parasites were cultivated at a density of $1x10^6$ per well in a 96-well black plate, using BHI medium (for epimastigotes) or RPMI medium (for trypomastigotes), with at least 7 concentrations of the compounds for 24 h. Fifty microliters of resazurin 2 mg/mL were added to each well, and the black plates were incubated for 4 h at 28°C (for epimastigotes) or 37°C (for trypomastigotes), shielded from light. Resazurin is reduced by mitochondrial NADH dehydrogenase to form resorufin, a highly fluorescent red compound. Fluorescence (λ_{ex} 530 nm/λ_{em} 590 nm) was measured

in a Thermo Scientific Varioskan® fluorimeter. $IC_{50,\ 24\ h}$ was determined from sigmoidal dose-response curves using GraphPad Prism version 8.00 for Windows. Results were presented as mean values ± standard deviation (SD) from three independent biological replicates. Nifurtimox was used as anti-*T. cruzi* reference drug.

2.4.2.3 Cytotoxicity in mammalian cells (VERO cells)

Cell viability on VERO cells after treatment with each compound was determined by MTT reduction assay. 1×10^3 cells were plated per well in 100 μL of RPMI medium in 96-well plates and incubated at 37°C with 5% CO_2 for 24 h to promote adherence. Different concentrations of each compound were added and incubated for 24 h. 20 μL of MTT solution (5 mg/mL in PBS) were added to each well and the plates were kept for 4 h at 37°C with 5% CO_2. After incubation, the medium was removed, 100 μL of DMSO were added to each well, and the plate was incubated for 15 min at room temperature with constant stirring, protected from light. Absorbance at 570 nm was monitored in a Thermo Scientific Varioskan Flash Multimode spectrophotometer and the IC_{50} values were extracted from the fitted sigmoidal curve. Dose-response curves were constructed using GraphPad Prism version 8.00 for Windows. The results were presented as the mean values ± standard deviation of three independent biological replicates (Rodriguez Arce et al., 2015).

2.4.3 *Trypanosoma cruzi in vitro* infection experiments

2.4.3.1 Impact on the infection process

The *in vitro* infection experiments were carried out as previously described for similar vanadium-based complexes (Scalese et al., 2019; Scalese et al., 2021). A total of 50,000 cells per well were seeded in a 24-well plate using RPMI medium and incubated at 37°C in a 5% CO_2 atmosphere until adherence occurred. Trypomastigotes derived from cells were collected from the supernatant of infected VERO cells 96 h post-infection. The parasites were treated for 30 min with the most selective compound of the series, $[V^{IV}O(L2\text{-}H)(mpo)]$, at concentrations equivalent to 1×, 5×, and 10× the previously determined $IC_{50,\ 24h}$ on *T. cruzi* cell-derived trypomastigotes. The treated parasites were used to infect the adhered VERO cells at a parasite-to-cell ratio of 10:1. After a period of incubation of 24 and 48 h, they were washed with PBS, fixed with 4% paraformaldehyde for 30 min, and stained with DAPI. Statistical analysis involved performing ANOVA tests with Bonferroni correction, analyzing twelve well plates, and evaluating eight independent fields for each experiment.

2.4.3.2 Influence on intracellular parasite's replication

In a 24-well plate, 50,000 infected cells were seeded per well. Following adherence, the infections were subjected to treatment with $[V^{IV}O(L2\text{-}H)(mpo)]$ for 24 and 48 h at concentrations equivalent to ×1, ×5, and ×10 the previously determined IC_{50} value for *T. cruzi* trypomastigotes at 24 h. After treatment, the cells underwent PBS washing, fixation with 4% paraformaldehyde for 30 min, and staining with DAPI. The quantification of amastigotes per cell was performed through direct counting. Each assay comprised three independent experiments, and a minimum of 40 cells were counted across eight randomly selected fields, amounting to approximately 300 cells per condition. This approach facilitated the evaluation of the percentage of infected cells following each treatment (Scalese et al., 2019; Scalese et al., 2021).

2.4.4 Metallomics

2.4.4.1 Vanadium uptaken by *Trypanosoma cruzi*

In order to estimate the amount of compound captured by the parasites, the total amount of uptaken vanadium and/or strongly bound to them (not removable by washing) as well as the amount of vanadium that remains in the culture medium, was quantified as previously described (Scalese et al., 2018; Scalese et al., 2019; Scalese et al., 2021). Epimastigotes were incubated at a density of 1×10^7 parasites/mL, with the compound $[V^{IV}O(L2\text{-}H)(mpo)]$ at concentrations corresponding to 1×, 5×, and 10× the previously determined $IC_{50,\ 24h}$ on trypomastigotes for 4 and 24 h. The supernatant (containing not uptaken compound) was separated from the parasites pellet by centrifugation for 10 min at 1,000 g. The pellet was washed with PBS and resuspended in 500 μL of PBS. The amount of vanadium in both fractions was measured by electrothermal atomic absorption spectrometry using a Thermo iCE 3500 spectrometer (Thermo Fisher Scientific) equipped with a graphite atomizer furnace. The optimal pyrolysis and atomization temperatures were 1,300 and 2,750 °C, respectively. A reference stock solution with a concentration of $1,000\ mg\ L^{-1}$ was prepared by dissolving $V^{IV}OSO_4 \cdot 5H_2O$ in 0.1% v/v nitric acid. The temperature program was optimized to achieve complete vaporization of the sample. The detection limit was $0.15\ \mu g\ L^{-1}$. The precision (expressed as % RSD) was greater than 5%. The accuracy of the method (expressed as percentage recovery) was 95–102%. Three independent experiments were conducted for each of the analyzed concentrations at different times. The percentage of vanadium captured by the parasites was determined according to the following equation: % entry = P/P + S, where P represents the amount (in ng) of vanadium determined in the parasite pellet, S the amount (in ng) of vanadium in the supernatant, and P + S the total amount (in ng) of the incorporated metal in the experiment.

2.4.4.2 Vanadium association with macromolecules

The amount of vanadium associated with DNA, RNA, soluble proteins (SP), and insoluble fraction (IF) containing insoluble proteins and membrane lipids among other insoluble molecules, was determined using electrothermal atomic absorption spectrometry (Scalese et al., 2018; Scalese et al., 2019; Scalese et al., 2021). Epimastigotes of *T. cruzi* were incubated at a density of $1x10^7$ parasites/mL for 24 h under the incubation conditions detailed in Section 2.4.4.1, identical to those used for the total vanadium uptaken. To separate soluble proteins from the insoluble fraction, 3×10^7 parasites were centrifuged and resuspended in parasite lysis buffer, containing 10 mM Tris-HCl pH 7.5, 1 mM EDTA, 1% CHAPS, 10% glycerol, 0.5% Triton, and a protease inhibitor (Complete™ Protease Inhibitor Cocktail-Roche). The mixture was shaken on ice for 30 min, and the lysate was centrifuged at 20,000 g for 1 h at 4°C. Soluble proteins were separated from the supernatant, and the insoluble fraction was separated from the lysate pellet, which was

resuspended in 0.5 mL of PBS for vanadium content determination. DNA was extracted using a FastDNA® Kit MPBio. The isolation of total RNA was carried out using Trizol reagent (Life Technologies) from an initial pool of 2×10^7 parasites. For each of the analyzed concentrations and various time points, three independent experiments were performed. The quantification of vanadium was performed for each fraction, and association percentages were calculated as follows: ng of vanadium in a specific macromolecule fraction divided by the total ng of vanadium. The total ng of vanadium is the sum of vanadium ng in the RNA fraction, vanadium ng in the DNA fraction, vanadium ng in the soluble protein fraction, and vanadium ng in the insoluble protein fraction.

2.4.5 Lipophilicity studies

Lipophilicity was experimentally determined using thin-layer chromatography (TLC) on reverse-phase TLC plates pre-coated with SIL RP-18W/UV$_{254}$ and eluted with a mixture of MeOH: DMF: Tris-HCl Buffer (10 mM), pH 7.4 (85:5:10, v/v/v). Ligand and complex solutions were prepared in MeOH immediately before use. The plates were run in a closed chromatography chamber, dried, and revealed under UV light. Reported R_M values represent the average of two to three determinations. R_M values were calculated using the relationship: $R_M = \log [(1/Rf) - 1]$ (Benitez et al., 2011; Fernandez et al., 2013a; Scalese et al., 2015; Scalese et al., 2018).

2.4.6 *Trypanosoma cruzi* death analysis
2.4.6.1 Parasites recovery experiments

To assess whether the vanadium compounds exert a trypanostatic or trypanocidal effect, recovery experiments were conducted by incubating *T. cruzi* epimastigotes at concentrations equivalent to 1×, 5×, and 10× the previously determined IC$_{50, 24h}$ on trypomastigotes for 24 h (Kessler et al., 2013). After the incubation period, the parasites were collected by centrifugation at 2000 *g* for 10 min, washed with fresh BHI medium, and transferred to fresh BHI medium devoid of the compound. Relative growth was evaluated by determining the ratio between the cell density of cultures incubated with the compound and control samples, following the optical density at 595 nm at incremental time points up to 7 days, and normalizing the data to the initial time point. Data were collected using a Thermo Scientific Varioskan® Flash Multimode spectrophotometer. The effect was considered trypanostatic if the parasites regained their normal growth, or trypanocidal in cases where growth arrest was irreversible. Assays were performed three times independently.

2.4.6.2 Cell death mechanism

The cell death mechanism induced by the most active compound [V^{IV}O(L2-H)(mpo)] was studied in the epimastigote form of *T. cruzi* employing the Dead Cell Apoptosis Kit (Thermo Fisher Scientific) and using the conditions that had been previously optimized for *T. cruzi* epimastigotes (Deolindo et al., 2005; Irigoin et al., 2009; Sandes et al., 2014; Veiga-Santos et al., 2014; Mosquillo et al.,

2018a; Mosquillo et al., 2018b). Briefly, the parasites were treated for 4 and 24 h at concentrations equivalent to ×1, ×5, and ×10 the previously determined IC$_{50, 24h}$ on trypomastigotes. After the incubation time, the parasites were harvested by centrifugation, washed with PBS, and resuspended in Annexin V binding buffer. Alexa Fluor 488-Annexin V (AV) (5 mg/mL) and propidium iodide (PI) (10 mg/mL) were added, and the mixture was incubated for 15 min at room temperature. The parasites were immediately analyzed using a flow cytometer BD Accuri C6 (BD Biosciences) with a collection flow rate of 100 μL/min. Fluorescence emission was measured with a 533/30 nm filter (FL1) for Annexin V and a 670 nm long pass filter (FL3) for PI, using a 488 nm excitation wavelength. A color compensation of 1.67% was applied (Mosquillo et al., 2018a; Mosquillo et al., 2018b). The data were analyzed using BD CSampler software (BD Bioscience). Untreated parasites were used as a negative control, and parasites treated with 50 μM and 100 μM H$_2$O$_2$ for 2.5 h served as positive controls for apoptosis and necrosis, respectively.

2.4.6.3 Reactive oxygen species generation

To evaluate whether the investigated compounds induce oxidative stress in parasites, we examined the production of reactive oxygen species (ROS) triggered by the specific compound, following a previously established protocol (Scalese et al., 2021). In brief, epimastigotes (1×10^7 parasites/mL) were cultured for 4 and 24 h with concentrations corresponding to 1×, 5×, and 10× the previously determined IC$_{50}$ value for trypomastigotes at 24 h. Subsequently, the parasites were exposed to 10 μg/mL H$_2$DCFDA (Thermo Fisher) in PBS for 1 h at 28 °C. As a positive control for ROS production, H$_2$O$_2$ (50 μM) was utilized. ROS levels were quantified using a Thermo Scientific Varioskan® Flash Multimode instrument with an excitation wavelength of 507 nm and an emission wavelength of 530 nm. Three independent experiments were conducted. The ANOVA test with Bonferroni correction was employed, analyzing twelve well plates and eight independent fields for each experiment.

2.4.6.4 Mitochondrial membrane potential assessment

To investigate changes in mitochondrial membrane potential (ΔΨm), we employed the lipophilic cationic marker, 5,5′,6,6′-tetrachloro-1,1′,3,3′-tetraethylbenzimidazol carbocyanine (JC1). This probe accumulates in a potential-dependent manner within the mitochondria, forming aggregates in healthy cells (red aggregates). In apoptotic cells, JC1 disperses, emitting fluorescence at lower wavelengths (green monomers). To assess the mitochondrial membrane potential, epimastigotes of *T. cruzi* (1×10^7 parasites/mL) were incubated with concentrations corresponding to 1×, 5×, and 10× the previously determined IC$_{50, 24h}$ on trypomastigotes, for 4 and 24 h. After the incubation period, the samples were incubated with the JC-1 probe at a final concentration of 6 μM for 30 min. Fluorescence intensities were measured (λ_{ex}= 560 nm/λ_{em}= 590 nm for red aggregates; λ_{ex}= 485 nm/λ_{em}= 530 nm for green monomers) using a Thermo Scientific Varioskan® Flash Multimode plate fluorometer (Mosquillo et al., 2018a; Mosquillo et al., 2018b).

2.4.7 *Trypanosoma cruzi* NADH-fumarate reductase (*Tc*FR) inhibition

2.4.7.1 *Tc*FR activity quantification

For *Tc*FR activity quantification, a protein extract was prepared from *T. cruzi* epimastigotes following a previously reported procedure (Vieites et al., 2008). Briefly, 3×10^7 parasites were harvested at 500 g and resuspended in MST buffer (0.23 M mannitol; 0.07 M sucrose; 5 mM Tris/HCl; pH 7.4), supplemented with protease inhibitor tablets (SIGMAFAST). Epimastigote cell suspensions were homogenized in the presence of 0.1% Triton X-100 surfactant and 200 mM KCl on ice using a Potter–Elvehjem Teflon-glass homogenizer, which was used to disrupt cell membranes and extract the enzyme. The extract was immediately used for the spectrophotometric assay of fumarate reductase enzyme activity, which depends on the rate of NADH oxidation at a wavelength of 340 nm, using a concentration of 250 μM NADH in HEPES buffer (30 mM, pH 7.0) with KCl (125 mM) and fumarate (0.5 mM) (Christmas and Turrens, 2000; Rodríguez Arce et al., 2015).

2.4.7.2 Computational modeling and simulation

2.4.7.2.1 DFT/PCM structural characterization of the [$V^{IV}O(L-H)(mpo)$] species.

The structure of each compound in water was obtained by full geometry optimization at the ωB97XD (Chai and Head-Gordon, 2008)/LANL2DZ (Hay and Wadt, 1985a; Hay and Wadt, 1985b)/6-31+G(d) (Ditchfield et al., 1971; Hariharan and Pople, 1973; Francl et al., 1982; Rassolov et al., 1998) level of theory using an ultrafine integration grid and representing the solution by the IEF-PCM (Tomasi et al., 1999) continuum model with a molecular-shaped cavity (atom centered Bondi's radii (Bondi, 1964) intersected spheres) and including non-electrostatic contributions [cavitation, repulsion, and dispersion terms (Pierotti, 1976; Floris and Tomasi, 1989; Floris et al., 1991)] as implemented in Gaussian16 rev C.01 (Frisch et al., 2019). All the species were verified to be stationary points (minima) on the corresponding potential energy surface through the analysis of the eigenvalues of the analytical Hessian.

2.4.7.2.2 Ligand-protein docking to *Tc*FR:NADH and molecular dynamics simulations.

The three-domain protein in the open conformation loaded with NADH cofactor [*Tc*FR:NADH 3D template (Salazar et al., 2023)] and the five compounds taken as ligands were configured (through AutoDockTools, ADT 1.5.4) using Autodock v4.2 (Morris et al., 2009) by adding any eventually missing hydrogen atoms and calculating Gasteiger charges (Gasteiger and Marsili, 1978; Gasteiger and Marsili, 1980) to perform biased docking using a grid centered on the NADH cofactor in the catalytic domain of 96x126x96 points per axis and spaced by 0.592 Å 500 runs were generated with the Lamarckian genetic algorithm (Morris et al., 1998; Fuhrmann et al., 2010) using the default settings with an initial population of 150 random individuals and maximum numbers of 2.5×10^6 and 2.7×10^4 energy evaluations and generations, respectively. Mutation and crossover rates were chosen to be 0.02 and 0.8. After a first inspection, torsion of dihedral angles in L2, L3, and L4 was restricted to achieve poses retaining the coordination sphere of V=O. Representative structures from the most populated conformational cluster of each NADH-TcFR:L 1:1 complexes were extracted and made available in PDB format to analyze the binding mode in detail. Binding free-energies (ΔG_{bind})

and dissociation constants ($K_d = e^{-\Delta G_{bind}/RT}$) are provided at T = 298 K both for the most populated and the most stable conformational clusters (Morris et al., 1998). Molecular dynamics simulations at 298 K and 1 atm were also conducted for 500 ns of production to confirm the stability of the complexes, introducing flexibility into the protein structure and NADH positioning (see Supporting Material for details and references on the protocol followed).

3 Results and discussion

3.1 Synthesis and characterization

The complexes [$V^{IV}O(L-H)(mpo)$], where L are the bioactive ligands derived from 8-hydroxyquinoline (L0-L4) and mpo is the deprotonated 2-mercaptopyridine *N*-oxide, were obtained by reacting $V^{IV}OSO_4$ with a stoichiometric amount of ligands in an aqueous basic medium. Throughout the procedure, inert atmosphere conditions were maintained to prevent oxidation of the central atom. Filtration, washing, and drying of the compounds were carried out using a continuous stream of N_2, and the solid was dried under vacuum. All compounds were obtained as brownish-green solids. Synthesis yields, expressed in mass and percentage, are provided in Supplementary Table S1. All the obtained complexes were characterized through elemental analysis, FTIR, and EPR spectroscopy. Additionally, the magnetic properties of the compounds were measured to confirm the metal oxidation state in the solid state. The number of hydration molecules was confirmed through TGA.

3.1.1 Characterization in the solid state

The proposed chemical formulas were confirmed through carbon, hydrogen, and nitrogen elemental analysis and TGA. The percentages obtained for each of these elements align with the theoretical values calculated based on the proposed formulae. For some compounds, water molecules were included to adjust the obtained percentage values. The number of water molecules included in the formulas was confirmed through TGA. Additionally, since the sample was burned in the presence of oxygen, the TGA allowed the calculation of the total amount of vanadium in the sample, assuming that the only final product is vanadium oxide V_2O_5 (Supplementary Table S2).

The coexistence of mpo ligands and derivatives of 8-hydroxyquinoline within the coordination environment of vanadium results in intricate FTIR spectra, especially within the $1{,}600^{-1}{,}500$ cm^{-1} range, where numerous bands associated with ν(C=C) in heterocyclic compounds manifest. These bands exhibit shifts to lower energies, which is indicative of ligand coordination to the metal center. To identify the presence of coordinated mpo in the complexes, bands associated with the ν(N-O), δ(N-O), and ν(C-S) vibrations of the *N*-oxide and thiol groups were identified. Supplementary Figure S1 shows an infrared spectrum obtained for [$V^{IV}O(L2-H)(mpo)$] compared to the free mpo and L2 ligands, and Supplementary Table S3 summarizes the tentative assignment of relevant bands in the IR spectrum for the mpo ligand present in all five complexes [$V^{IV}O(L-H)(mpo)$]. The spectral profile was similar for all compounds. Due to coordination,
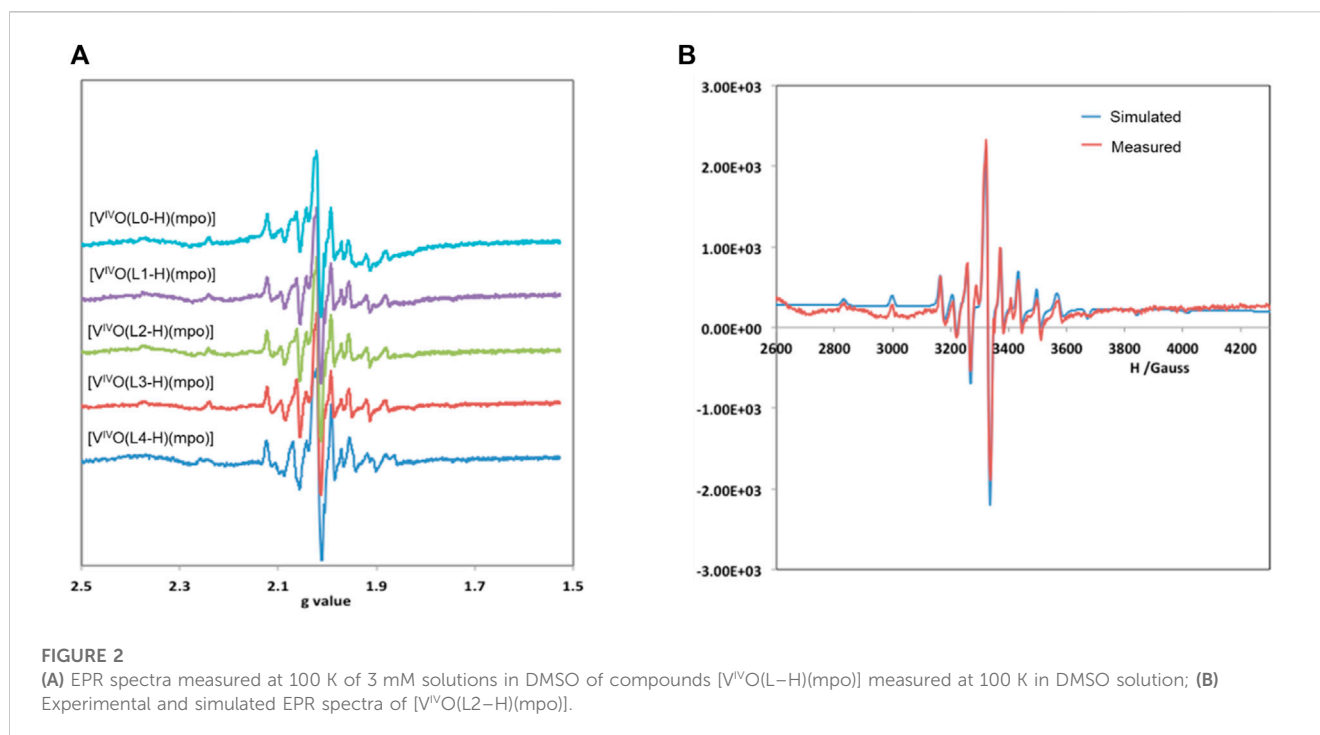
FIGURE 2
(A) EPR spectra measured at 100 K of 3 mM solutions in DMSO of compounds [V^{IV}O(L−H)(mpo)] measured at 100 K in DMSO solution; **(B)** Experimental and simulated EPR spectra of [V^{IV}O(L2−H)(mpo)].

a shift in the ν(N-O) and ν(C-S) bands of mpo was observed. The shift is consistent with the bidentate coordination of mpo through the sulfur atom and the oxygen of the *N*-oxide group (Vieites et al., 2008; Vieites et al., 2009; Machado et al., 2014; Rodriguez Arce et al., 2015). In all complexes, an intense band corresponding to ν(V=O) at around 968 cm^{-1}, characteristic of the V^{IV}O^{2+} center, was identified.

3.1.2 Characterization in solution

The molar conductivity, measured in 1 mM solutions in DMSO for all the new complexes, ranged from ~1 to 3 S cm^2/mol. The obtained values indicate that these are neutral compounds, in agreement with the proposed [V^{IV}O(L-H)(mpo)] formulas.

The complexes were also characterized in solution using EPR spectroscopy. Solutions of the complexes were prepared at concentrations of 3 mM at room temperature in DMSO that had been previously degassed by bubbling N$_2$ for 10 min. EPR spectra were immediately recorded at 100 K (Figure 2A), and spin Hamiltonian parameters were obtained through simulation using the program developed by Rockenbauer and Korecz (Table 1) (Rockenbauer and Korecz, 1996). As an example, Figure 2B shows the comparison between the measured and simulated EPR spectrum for [V^{IV}O(L2-H)(mpo)]. Due to the low signal intensity obtained for the [V^{IV}O(L0-H)(mpo)] spectrum, this spectrum was not simulated.

All the studied oxidovanadium(IV) complexes exhibit an EPR spectrum with a characteristic hyperfine pattern indicative of monomeric vanadium compounds in the oxidation state (IV). The results confirm the same coordination mode for all complexes involving both ligands in the equatorial plane. In fact, using the additivity rule ($|A_z^{est}| = \Sigma|A_{zi}|$ (i=1–4), where $|A_{zi}|$ is the contribution of each of the donor atoms in the equatorial plane), the value $|A_z^{est}| = 153.5 \times 10^{-4}$ cm^{-1} was obtained, which is consistent with the coordination through two aromatic O-atoms, the pyridinic

TABLE 1 Spin Hamiltonian parameters obtained by simulation of the experimental EPR spectra in DMSO measured at *ca*. 100 K.

Compound	g$_{x,y}$	g$_z$	A$_{x,y}$ (x10^{-4} cm^{-1})	A$_z$ (x10^{-4} cm^{-1})
[V^{IV}O(L1-H)(mpo)]	1.984	1.959	52.3	154.6
[V^{IV}O(L2-H)(mpo)]	1.981	1.958	53.0	155.4
[V^{IV}O(L3-H)(mpo)]	1.983	1.958	53.3	155.6
[V^{IV}O(L4-H)(mpo)]	1.983	1.957	53.3	155.9

nitrogen, and the aromatic sulfur (2 x Ar-O, N$_{pyr}$, Ar-S) (Wüthrich, 1965; Chasteen, 1981; Smith et al., 2002; Micera et al., 2009; Sanna et al., 2012).

The EPR spectra measured immediately after dissolution decreased in intensity compared to those measured in the solid state, indicating the rapid oxidation of the species upon dissolution. The oxidation is evident in the ^{51}V NMR spectra, where signals appear around −450 ppm (Supplementary Figure S2A). These signals can be assigned to an oxidized species of the compound with both ligands coordinated, [V^{V}O(L-H)(mpo)], as the homoleptic species {V^{V}O(L-H)$_2$} is expected to have a chemical shift close to −470 ppm (Correia et al., 2014; Scalese et al., 2022). After 21 h, a second signal centered at −482 ppm appears. This behavior is similar to that found in some homoleptic series of oxidovanadium(IV) complexes with L0-L4 ligands (Correia et al., 2014; Scalese et al., 2019). This signal can be assigned to solvolysis products obtained upon the oxidation of the V^{IV}-center, V^V-L complexes being formed in solution. These findings are corroborated by the UV-Vis spectra obtained under identical conditions for the complex [V^{IV}O(L2-H)(mpo)]

(Supplementary Figure S2B). Shoulders around 550 and 700 nm in the spectrum, overlaying highly absorptive charge transfer bands due to the presence of the coordinated organic ligands, can be attributed to d-d transitions of the V(IV) center. The highly absorptive UV bands are clearly observed in the spectrum of the solution of the complex upon dilution 1:10 (depicted by the yellow-brown line in Supplementary Figure S2B). Even after 21 h, the d-d bands remain observable, albeit with a diminished intensity, aligning with the previously mentioned partial oxidation.

We should highlight that the solutions corresponding to the spectra of Figure 2, and Supplementary Figures S2A, S2B are quite concentrated (3 mM), and it is plausible to expect that in water containing solvents and at lower concentrations, the relative amount of V^V-species and extent of hydrolysis will be significantly higher. In fact, several publications have reported that metal complexes of labile metal ions, such as those of Cu(II) and oxidovanadium(IV), once in aqueous solution, and particularly at low concentrations and/or in biological media, may undergo hydrolysis, oxidation (case of V^{IV}-complexes) and/or ligand exchange (Levina et al., 2017; Levina and Lay, 2017; Nunes et al., 2020; Nunes et al., 2021; Pessoa and Correia, 2021). This is relevant here to explain the ^{51}V NMR data and for the next sections to fully explain the biological results.

3.2 Biological results

3.2.1 *In vitro* activity against *Trypanosoma cruzi* and *Leishmania infantum* and selectivity towards the parasites

The five complexes were evaluated *in vitro* for their antiparasitic activity against *T. cruzi* and *L. infantum*. Firstly, the compounds were evaluated on the non-infective epimastigote form of *T. cruzi* and the axenic promastigote form of *L. infantum*, determining the IC_{50} values after 5 days of treatment (IC_{50}, 5 days). In parallel, unspecific cytotoxicity was studied on VERO cells as a mammalian cell model to evaluate the selectivity towards the parasites. The results were compared to those of the free ligands and the reference drugs Nifurtimox and Amphotericin B (Table 2).

The novel complexes inhibit the growth of both parasites in the micromolar and submicromolar range (IC_{50}, 5 days, *T. cruzi* = 0.33–3.39 μM/IC_{50}, 5 days, *L. infantum* = 0.65–1.56 μM), with IC_{50} values of the same order or even lower than the reference drugs. Almost all the complexes showed similar or higher activity than the free L ligands on *T. cruzi* epimastigotes and trypomastigotes, and *L. infantum* promastigotes. Interestingly, for *T. cruzi*, complexes with ligands substituted at positions 5 and 7 of the 8-hydroxyquinoline moiety showed IC_{50}, 5 days values lower than Nifurtimox. However, they show IC_{50}, 5 days somewhat higher than Amphotericin B against *L. infantum*.

As previously reported for the 8-hydroxyquinoline derivatives and the homoleptic series $[V^{IV}O(L-H)_2]$ and $[V^VO(OCH_3)(L-H)_2]$ (Scalese et al., 2019), *T. cruzi* was more sensitive to the new vanadium compounds than *L. infantum*.

The five new heteroleptic oxidovanadium(IV) compounds also showed activity against both stages of *T. cruzi* in the micromolar and submicromolar range when they were exposed for 24 h. The IC_{50}, 24 h values (Table 2) were very similar to the IC_{50}, 5 days values determined over 5 days for *T. cruzi* and *L. infantum* (IC_{50}, 24 h, epimastigotes = 0.83–4.36 μM/IC_{50}, 24 h, trypomastigotes = 0.19–1.00 μM) (Table 2). As observed in previous series, when changing the incubation time, the IC_{50}, 24 h values for the epimastigote form were 1.2–2.7 times higher than the previously discussed IC_{50}, 5 days values. The trypomastigote form proved to be 2 to 4 times more sensitive to the compounds $[V^{IV}O(L-H)(mpo)]$ than the epimastigote form.

The IC_{50}, 24h and selectivity index values obtained indicate that the $[V^{IV}O(L-H)(mpo)]$ series turned out to be more toxic than the previously developed homoleptic compounds, as their IC_{50} values in the model mammalian cells also fall in the micromolar range (Table 2). The homoleptic compound $[V^{IV}O(mpo)_2]$, previously developed as an insulin-mimetic compound, does not show high toxicity (IC_{50} fibroblasts NCTC/IC_{50} *T. cruzi* = 61) (Gambino, 2011), which suggests that toxicity of these compounds might be associated with the inclusion of the 8-hydroxyquinoline fragment in the coordination sphere.

Interestingly, while the selectivity index values are low, a pattern of increased selectivity for complexes with halogen-substituted ligands can be recognized. It is noteworthy that, like what happens with $[V^{IV}O(L0-H)_2]$ and $[V^{IV}O(L0-H)_2(OCH_3)]$, the complex $[V^{IV}O(L0-H)(mpo)]$ presents an equal IC_{50} value against *T. cruzi* as against VERO cells. Despite the significant toxicity found for some of these complexes, in this series, $[V^{IV}O(L1-H)(mpo)]$ and $[V^{IV}O(L2-H)(mpo)]$ have acceptable selectivity values when comparing the activity in the trypomastigote form with the cytotoxicity in VERO cells (>10) (Katsuno et al., 2015). Being $[V^{IV}O(L2-H)(mpo)]$ the most promising compound in *T. cruzi*, it was selected for further biological studies. In order to facilitate a comprehensive comparison of the results, the experiments were carried out using compound concentrations equivalent to 1×, 5×, and 10× the IC_{50}, 24 h value previously determined in cell-derived trypomastigotes (0.67 μM, 3.35 μM y 6.70 μM, respectively).

3.2.2 Effects on the *Trypanosoma cruzi* infection ability and the replication of intracellular amastigotes

Exploration of the effect of the selected oxidovanadium compound, $[V^{IV}O(L2-H)(mpo)]$, on the infection ability of the parasite, was undertaken. Trypomastigotes derived from cells were exposed to varying concentrations of the $V^{IV}O$ compound (1×, 5×, and 10× the previously determined IC_{50}, 24 h value on cell-derived trypomastigotes, shown in Table 2). Subsequently, these pre-treated trypomastigotes were employed to infect VERO cells. The quantification of infected cells after 24 and 48 h for each treatment was compared with control cells infected with untreated trypomastigotes (see Figure 3A). A statistically significant reduction in the percentage of infected cells was observed at both tested time points. The results obtained for concentrations equivalent to 1×, 5×, 10×

TABLE 2 *In vitro* activity of [$V^{IV}O(L-H)(mpo)$] compounds against *T. cruzi* (CL Brener strain, epimastigotes and trypomastigotes) and *L. infantum* (MHOM MA67I7MAP263 strain promastigotes), cytotoxicity in model mammalian cells (VERO cells, ATCC CCL81), and selectivity index values against parasites (SI).

Compound	$IC_{50, 24h}$ VERO cells ± SD (µM)	$IC_{50, 5\,days}$ promastigotes *L. infantum* ± SD (µM)	SI^a	$IC_{50, 5\,days}$ epimastigotes *T. cruzi* ± SD (µM)	SI^b	$IC_{50, 24\,h}$ epimastigotes *T. cruzi* ± SD (µM)	SI^c	$IC_{50, 24\,h}$ trypomastigotes *T. cruzi* ± SD (µM)	SI^d
Nifurtimox	998.5 ± 90.6[e]	ND	ND	2.76 ± 0.19[g]	361	3.68 ± 0.71[f]	271	20.10 ± 2.86[f]	49.6
Amphotericin B	>100[e]	0.55 ± 0.07[e]	>182	ND	ND	ND	ND	ND	ND
L0	10.1 ± 3.9[g]	0.73 ± 0.15	13.8	5.5 ± 0.5[g]	1.8	9.42 ± 2.23[f]	1.1	0.47 ± 0.07[f]	21.5
L1	66.5 ± 13.1[e]	2.65 ± 0.37[e]	25.1	0.31 ± 0.01[e]	214	7.17 ± 1.07[f]	9.3	2.25 ± 0.95[f]	29.5
L2	64.7 ± 9.1[e]	3.20 ± 1.40[e]	20.2	1.04 ± 0.09[e]	62.2	2.56 ± 0.52[f]	23.4	0.40 ± 0.08[f]	162
L3	75.5 ± 16.3[e]	2.22 ± 0.09[e]	34.0	1.41 ± 0.35[e]	53.5	2.17 ± 0.35[f]	34.8	1.10 ± 0.88[f]	68.6
L4	12.5 ± 4.5[e]	2.36 ± 0.04[e]	5.3	1.77 ± 0.72[e]	7.1	2.58 ± 0.56[f]	4.8	1.01 ± 0.73[f]	12.3
Na mpo	21.2 ± 2.7	0.93 ± 0.11	22.8	0.48 ± 0.026	44.2	1.45 ± 0.51	15.0	0.26 ± 0.04	83.8
[$V^{IV}O(L0-H)(mpo)$]	4.99 ± 0.65	1.56 ± 0.75	3.2	3.39 ± 0.81	1.5	4.36 ± 1.50	1.1	1.00 ± 0.23	5.0
[$V^{IV}O(L1-H)(mpo)$]	9.68 ± 0.95	0.65 ± 0.32	14.9	0.65 ± 0.044	14.9	3.89 ± 1.94	2.5	0.88 ± 0.13	10.1
[$V^{IV}O(L2-H)(mpo)$]	14.9 ± 2.1	0.80 ± 0.05	18.6	2.13 ± 0.21	7.0	1.74 ± 0.37	8.5	0.67 ± 0.21	22.1
[$V^{IV}O(L3-H)(mpo)$]	2.32 ± 0.32	1.38 ± 0.10	1.7	1.45 ± 0.17	1.6	1.88 ± 0.70	1.2	0.91 ± 0.18	2.5
[$V^{IV}O(L4-H)(mpo)$]	1.35 ± 0.30	1.30 ± 0.34	1.0	0.33 ± 0.014	4.1	0.83 ± 0.06	1.6	0.19 ± 0.03	7.1

[a]$IC_{50, 24\,h}$ VERO/$IC_{50, 5\,days}$ promastigotes *L. infantum*.
[b]$IC_{50,24\,h}$ VERO/$IC_{50, 5\,days}$ epimastigotes *T. cruzi*
[c]$IC_{50,24\,h}$ VERO/$IC_{50, 24\,h}$ epimastigotes *T. cruzi*
[d]$IC_{50,24\,h}$ VERO/$IC_{50, 24\,h}$ trypomastigotes *T. cruzi*
[e]Data from reference (Scalese et al., 2019).
[f]Data from reference (Scalese et al., 2021).
[g]Data from reference (Scalese et al., 2018).
ND: not determined.
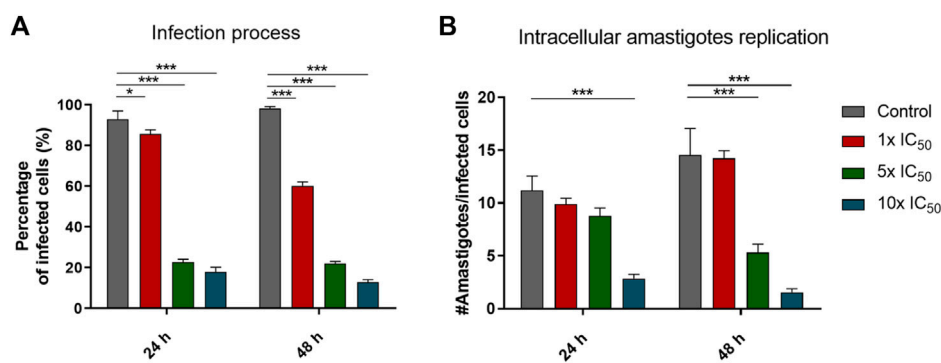
FIGURE 3
(A) Percentage of infected cells using parasites pre-treated with [$V^{IV}O(L2\text{-}H)(mpo)$]. The percentage of infected cells was compared against the control of cells infected with untreated trypomastigotes using a two-way ANOVA test. **(B)** Number of amastigotes per cell after 24 and 48 h of incubation with concentrations of the compound relative to the $IC_{50,24h}$ on cell-derived trypomastigotes of [$V^{IV}O(L2\text{-}H)(mpo)$]. Each condition is represented as the mean and standard deviation (SD). Three independent experiments were conducted, with a minimum of 300 cells counted for each experiment. ANOVA Test: * = $p < 0.05$, *** = $p < 0.001$.

TABLE 3 Percentages of vanadium uptaken by epimastigotes of *Trypanosoma cruzi* after incubating with [$V^{IV}O(L2\text{-}H)(mpo)$].

Compound concentration (μM)[b]	Vanadium uptaken (ng/10^7 parasites) ± SD		% entry[a] ± SD	
	4 h	24 h	4 h	24 h
1× $IC_{50,\ 24h}$−0.67	3.9 ± 0.3	6.3 ± 0.3	1.4 ± 0.1	2.2 ± 0.1
5× $IC_{50,\ 24h}$−3.35	15.6 ± 2.8	19.9 ± 2.8	1.1 ± 0.2	1.4 ± 0.2
10× $IC_{50,\ 24h}$−6.70	28.4 ± 2.8	31.3 ± 2.8	1.0 ± 0.1	1.1 ± 0.1

[a]% entry: Percentage of vanadium incorporated by the parasite (in the pellet) with respect to the total vanadium included in the parasite culture.
[b]Determination of IC_{50} values on *T. cruzi* trypomastigotes, as outlined in the Materials and Methods section.

the $IC_{50,\ 24\ h}$ of [$V^{IV}O(L2\text{-}H)(mpo)$] are similar to those reported for the multifunctional compounds [M(dppf)(mpo)], where M = Pd or Pt, which lead to a reduction in the percentage of infected cells by more than 80% (Mosquillo et al., 2018a; Mosquillo et al., 2018b). Comparing the results with those obtained for [$V^{IV}O(L1\text{-}H)_2$] (Scalese et al., 2019) and [$V^VO(IN\text{-}2H)(L2\text{-}H)$] (Scalese et al., 2021), where IN is 2-hydroxy-1-naphtaldehyde isonicotinoyl hydrazone, the findings suggest that the inclusion of the mpo ligand in the coordination compound results in a decrease in the infection capacity of the treated trypomastigotes.

Furthermore, to assess the influence of the vanadium compound on intracellular amastigote proliferation, we treated pre-established infections with concentrations of 1×, 5×, and 10× the previously determined $IC_{50,\ 24\ h}$ value on cell-derived trypomastigotes. We directly counted the number of amastigotes per infected cell after 24 and 48 h for each treatment (Figure 3B). The number of amastigotes per cell significantly decreases after a 24 h incubation with 10 times the previously determined $IC_{50,\ 24\ h}$ value on cell-derived trypomastigotes. In the case of the 48 h incubation, the decrease becomes significant for 5 times and 10 times the $IC_{50,\ 24\ h}$ value. This finding implies that the compound [$V^{IV}O(L2\text{-}H)(mpo)$], in the same way, that the previously reported [M(dppf)(mpo)] compounds, not only

impacts the infection process itself but also hinders the intracellular amastigotes' ability to multiply.

3.2.3 Metallomics studies in *Trypanosoma cruzi*
3.2.3.1 Vanadium uptaken by the parasites
To assess the compound's uptake by parasites, we quantified the total vanadium content absorbed or strongly bound to them (not removable by washing). This was then compared to the amount of vanadium remaining in the culture medium. Epimastigotes were exposed to [$V^{IV}O(L2\text{-}H)(mpo)$] for 4 and 24 h at concentrations corresponding to 1×, 5×, 10× the previously established IC_{50} value for trypomastigotes derived from cell cultures (0.67 μM, 3.35 μM, and 6.70 μM, respectively). The average vanadium content, determined over three independent experiments, is presented in Table 3. As expected, an increase in total uptaken vanadium was determined when parasites were incubated with higher compound concentrations. However, no significant differences in the % of uptaken vanadium were observed between incubation times of 4 and 24 h.

Overall, the vanadium incorporation percentage for the selected compound resulted low when compared to other complexes reported by us, such as [$V^VO(L0\text{-}H)(LS1\text{-}2H)$] (Scalese et al., 2018), where LS is the tridentate 2-hydroxy-1-naphthaldehyde semicarbazone derivative, [$V^{IV}O(L1\text{-}H)_2$] (Scalese et al., 2019), [$V^VO(IN\text{-}2H)(L2\text{-}H)$] (Scalese et al.,
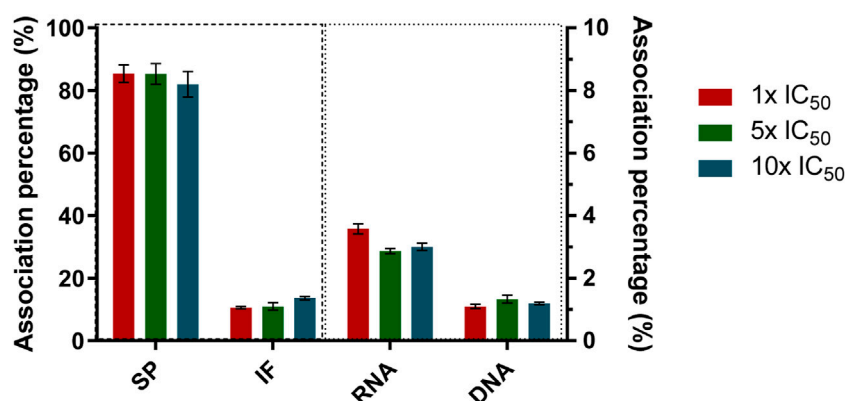
FIGURE 4
Percentage of vanadium associated with the different macromolecules isolated from *T. cruzi* epimastigotes after 24 h of incubation with 1×, 5×, 10× the IC$_{50, 24 h}$ previously determined on cell-derived trypomastigotes for [V^{IV}O(L2-H)(mpo)]. The mean value and standard deviation obtained from three independent experiments of association with DNA, RNA, soluble protein (SP), and insoluble fraction (IF) are shown.

2021), where IN is 2-hydroxy-1-naphtaldehyde isonicotinoyl hydrazone and the previous hit compound [V^{IV}O(LS2-2H)(NN)], with LS2 = 5-bromosalicylaldehyde semicarbazone and NN = 5-aminophenanthroline (Mosquillo et al., 2020b).

3.2.3.2 Association with parasite macromolecules

To investigate the subcellular distribution of the uptaken vanadium, the metal associated with macromolecules was determined after incubating epimastigotes for 24 h with [V^{IV}O(L2-H)(mpo)] at concentrations equivalent to 1×, 5×, 10× the previously determined IC$_{50, 24 h}$ value on cell-derived trypomastigotes (0.67 µM, 3.35 µM y 6.70 µM, respectively). After incubation time, macromolecular fractions (DNA, RNA, and proteins) were isolated. The total vanadium content associated with each fraction was quantified using electrothermal atomic absorption spectrometry (Figure 4).

The distribution analysis at the working conditions shows an association pattern very similar to those found for previously published oxidovanadium complexes with 8HQ derivatives: [V^{V}O(L0-H)(LS1-2H)] (Scalese et al., 2018), where LS1 is the tridentate 2-hydroxy-1-naphthaldehyde semicarbazone derivative, for [V^{IV}O(L1-H)$_2$] (Scalese et al., 2019) and for [V^{V}O(IN-2H)(L2-H)] (Scalese et al., 2021), where IN is 2-hydroxy-1-naphtaldehyde isonicotinoyl hydrazone. Particularly, an association close to 87% to soluble proteins was found, independently of the initial incubation concentration (Figure 4). This might be an indication that V-8HQ type species might be involved in the uptake and/or binding to biologically relevant molecules. The preferential binding of V-species to proteins is also in agreement with the belief that interference with the role of proteins may be relevant to the biological action of vanadium (Costa Pessoa et al., 2015; Pessoa et al., 2021; Santos et al., 2022; Ferraro et al., 2023). On the other hand, the amount of vanadium determined in the insoluble protein fraction is lower than that determined in the soluble fraction, which is, in this case, close to 13%. Less than 4% was found associated with nucleic acids, suggesting that the association with DNA and RNA is very low and that these

biomolecules are not considered potential targets. Although a similar association pattern was observed in the current and previous systems, the different percentages found for each fraction suggest that the nature of the ligands has a significant impact on the subcellular distribution. Namely, V^{IV}- and V^{V}-8-hydroxyquinoline species may be relevant in this respect (Ferraro et al., 2023).

3.2.4 Lipophilicity

Lipophilicity is one of the primary factors governing passage through the cell membrane, making it of great importance in studying the biological effects of potential pharmaceuticals. Lipophilicity was determined experimentally using reverse-phase TLC, simulating the hydrophobic lipids of cell membranes and biological receptors, and eluted with a mixture of MeOH: DMF: Tris-HCl Buffer, pH 7.4, which mimics the hydrophilic environment. Table 4 summarizes the measured Rf values and the calculated R_M values for all complexes and free ligands under the same experimental conditions. The [V^{IV}O(L-H)(mpo)] compounds showed slightly higher lipophilicity values compared to the free 8-hydroxyquinoline-derived ligands. As expected, the halo-substituted complexes are more lipophilic than the L0 complex, which may be correlated with the increase in antiparasitic activity. However, it is worth noting that compound [V^{IV}O(L4-H)(mpo)] stands out as an outlier in this tendency due to its significantly high toxicity in both parasites and mammalian cells, despite its lower experimentally determined lipophilicity.

3.2.5 Cell death assays
3.2.5.1 *Trypanosoma cruzi* recovery assays

Recovery experiments were performed on *T. cruzi* epimastigotes to determine whether the V^{IV}O-complex demonstrates a trypanostatic or trypanocidal impact on the epimastigote form. If the parasites resumed growth after 120 h in fresh medium, the compound was categorized as trypanostatic; however, it was considered trypanocidal if it resulted in an irreversible interruption of cell growth. The behavior of [V^{IV}O(L2-H)(mpo)]

TABLE 4 R_f and R_M values for ligands and complexes were determined using a mobile phase consisting of a mixture of MeOH:DMF:Tris-HCl Buffer (10 mM), pH 7.4 (85:5:10, v/v/v).

Compound	R_f	R_M
L0	0.85	−0.77
L1	0.81	−0.63
L2	0.79	−0.58
L3	0.53	−0.044
L4	0.89	−0.91
[$V^{IV}O$(L0-H)(mpo)]	0.76	−0.50
[$V^{IV}O$(L1-H)(mpo)]	0.75	−0.48
[$V^{IV}O$(L2-H)(mpo)]	0.73	−0.43
[$V^{IV}O$(L3-H)(mpo)]	0.72	−0.41
[$V^{IV}O$(L4-H)(mpo)]	0.76	−0.50

R_M, $\log_{10}[(1/R_f)-1]$ (Benitez et al., 2011; Fernandez et al., 2013a; Scalese et al., 2015; Scalese et al., 2018); ND, not determined.

FIGURE 5
Wash out experiments in BHI-Tryptose culture medium after incubation with [$V^{IV}O$(L2-H)(mpo)] for 24 h. Each experiment was conducted in triplicate, and each data point represents the average value and its standard deviation.
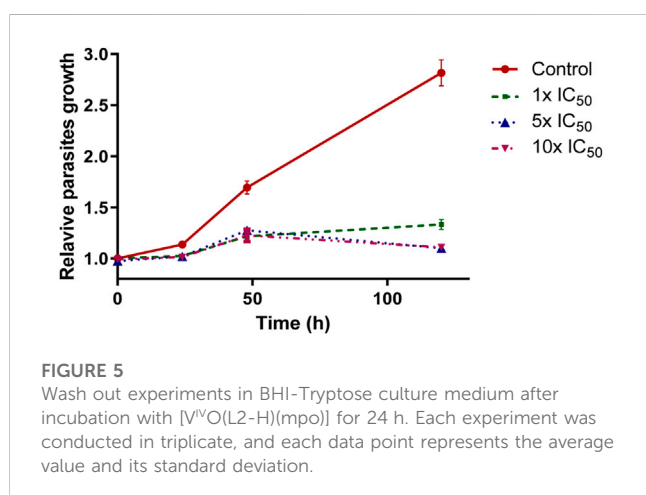
contrasts with observations made for previously developed oxidovanadium complexes featuring 8-hydroxyquinoline derivatives (Scalese et al., 2018; Scalese et al., 2019; Scalese et al., 2021). As illustrated in Figure 5, at all working concentrations, the parasites are unable to resume normal growth when transferred to a fresh compound-free medium. After 48 h, the parasites begin to die off. These results suggest a trypanocidal action by the selected compound under the analyzed conditions.

3.2.5.2 Parasites death mechanism

Since a trypanocidal effect was observed at all three analyzed compound concentrations (Figure 5), the mechanism associated with the death of the parasites was investigated. This analysis involved the use of fluorescent probes Annexin V (AV) and propidium iodide (PI) to distinguish between early apoptotic and necrotic/late apoptotic parasites, respectively, as previously described in the literature (Mosquillo et al., 2018a; Mosquillo et al., 2018b). Figure 6A shows the dot plot from flow cytometry

analysis of labeled AV/IP parasites after incubating with different concentrations of [$V^{IV}O$(L2-H)(mpo)] for 4 and 24 h. Induction of the apoptotic cascade was observed in the first 4 h of treatment, with a higher percentage of AV+/IP- parasites observed at higher compound concentrations (reaching 40% of cells). After 24 h of incubation, the number of double-labeled parasites AV+/IP+, corresponding to necrotic/late apoptotic cells, increased, reaching values of 16% of the total population at higher concentrations. Figure 6B graphically shows the observed concentration-dependent response after 24 h of incubation, where an increase in both apoptosis and necrosis was observed at higher concentrations. It should be noted that the percentage of the sum of apoptotic and necrotic cells observed after treatment with the compound concentration corresponding to 1× IC_{50} for 24 h, reaches only 39% which suggests the involvement of an alternative mechanism of cell death.

3.2.5.3 Oxidative stress and integrity of mitochondrial membrane potential

Depending on the levels of ROS produced, different mechanisms of cell death can be activated. On one hand, the mitochondrial defense response can lead to Ca^{2+} overload, which can induce apoptosis (Menna-Barreto, 2019; Docampo and Vercesi, 2022). One of the regulators of ROS-dependent cell death is the mitochondrial permeability transition pore. When parasites are exposed to hydrogen peroxide, there is a loss of mitochondrial membrane potential and lipid peroxidation, leading to necrosis (Bustos et al., 2017; Menna-Barreto, 2019). On the other hand, elevated levels of ROS have been found in parasites where the effect of mitochondrial membrane integrity on the formation of autophagosomes has been studied (Williams et al., 2012). The generation of ROS induced by vanadium compounds as a mechanism for cell death activation has been explored previously, primarily in tumor cells (Kowalski et al., 2020). Higher levels of ROS have been detected for complexes containing vanadium in the IV oxidation state as the central metal (Wu et al., 2016). The balance of mitochondrial membrane potential is crucial for ATP production by ATP synthase and for the transport of proteins into the mitochondria. Therefore, variations in this potential can be used as a marker for programmed cell death in mammals and protozoa (Genes et al., 2011). It has also been suggested that the mechanism of cell death depends on the degree of mitochondrial dysfunction. In cases where massive mitochondrial dysfunction compromising ATP supply is observed, cell death results in necrosis, whereas a milder form of mitochondrial dysregulation leads to apoptosis (Kroemer, 1997; Zamzami et al., 1997).

To investigate whether the new synthesized compounds induce the generation of ROS and if this phenomenon can be linked to the activation of the various discussed cell death mechanisms in *T. cruzi*, the probe 2′,7′-dichlorodihydrofluorescein diacetate (H_2DCFDA) was used. The effect of the compounds on mitochondrial membrane potential (Δψm) was assessed using the cationic probe JC1. After 4 h of treatment, there is a trend towards an increase in ROS levels as the complex concentration increases, although it does not reach statistical significance. However, regardless of the initial inoculation concentration, ROS levels significantly increase after 24 h compared to the control group (Figure 7A). After 24 h of exposure at concentrations corresponding to 10× $IC_{50, 24 h}$, the
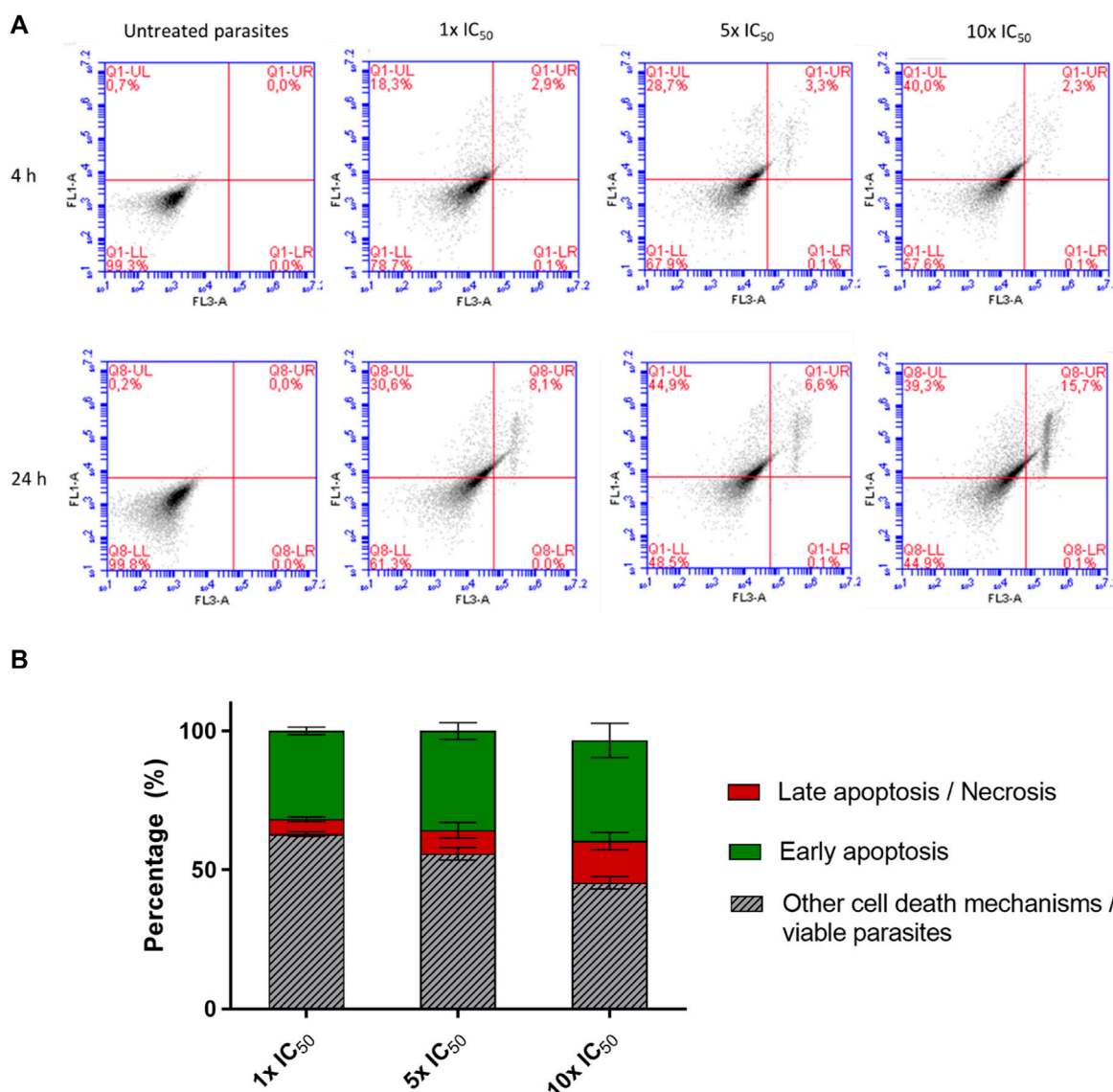
FIGURE 6
(A) Examination of the mode of cell death induced by [V^{IV}O(L2-H)(mpo)] in *T. cruzi* epimastigotes involved incubating parasites with concentrations corresponding to 1×, 5×, 10× the IC$_{50}$ for 4 and 24 h. They were labeled with fluorescent probes AV and IP to distinguish early apoptosis from late apoptosis/necrosis processes. Untreated parasites served as the control. The analysis was conducted using an Accuri C6 flow cytometer (BD Bioscience), where the X-axis represented regions labeled with IP (FL1 detector), and the Y-axis represented regions labeled with AV (FL3 detector). The upper right corner of the dot plots depicted the double-labeled area, while the lower left corner delineated the region occupied by unlabelled parasites. **(B)** Percentages of parasites labeled with the AV and IP after 24 h of treatment with 1×, 5×, 10× the IC$_{50, 24 h}$. The mean and standard deviation for three independent experiments is presented.

fluorescence rate decreased by 18–26%, significantly differing from the untreated parasite control. These results indicate that Δψm is compromised in treated parasites (Figure 7B). The observed changes in mitochondrial membrane potential, and hence the degree of mitochondrial dysfunction, may be linked to the presence of radical species that induce oxidative stress, affecting mitochondrial function (Docampo, 1990). When the depolarization results are considered in conjunction with the generation of ROS, it is evident that the behavior regarding radical species formation and mitochondrial membrane depolarization is similar (Figure 7).

In this case, the effect on mitochondrial membrane integrity suggests moderate dysregulation, which would indicate the induction of mitochondria-dependent apoptosis. Consistently, the compound analyzed showed a certain percentage of apoptotic cells, being this the primary mechanism of death. The mitochondrial membrane depolarization is not the only signaling mechanism that triggers cell death (Kroemer, 1997; Zamzami et al., 1997). So, it is postulated that the portion of necrotic parasites found may not have activated this cell death pathway due to mitochondrial dysfunction.
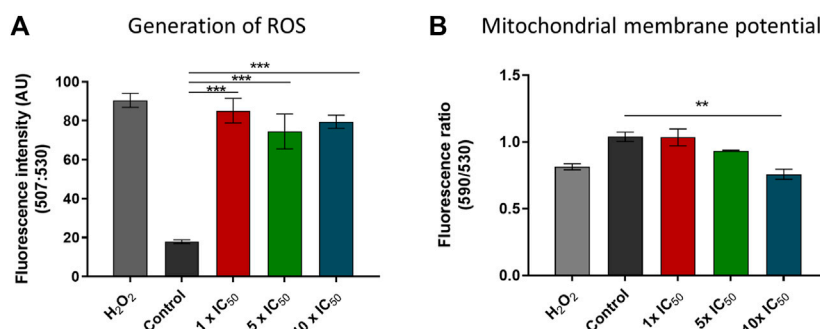
FIGURE 7
(A) ROS produced in *T. cruzi* epimastigotes after 24 h of treatment with [V^{IV}O(L2-H)(mpo)] at concentrations corresponding to 1×, 5×, 10× the IC$_{50, 24 h}$ previously determined on cell derived trypomastigotes. **(B)** The red/green fluorescence intensity ratio (590/530 nm) after 24 h of treatment with [V^{IV}O(L2-H)(mpo)] at concentrations corresponding to 1×, 5×, 10× the IC$_{50, 24 h}$ previously determined on cell derived trypomastigotes. Untreated parasites were used as a control. H$_2$O$_2$ 50 μM was used as a positive control. Fluorescence intensities at 590 and 530 nm were measured using a Varioskan Flash Spectral Scanning plate fluorometer. The average value and standard deviation are presented for each condition. Three independent experiments were conducted. ANOVA analysis: ** = $p < 0.01$*** = $p < 0.001$.
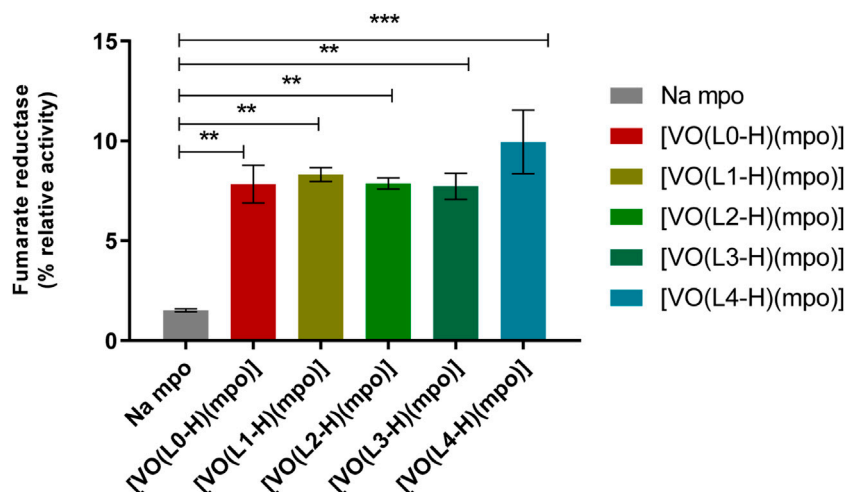
FIGURE 8
Impact of [V^{IV}O(L-H)(mpo)] compounds, where L = L0-L4, and the free ligand mpo on *Tc*FR enzyme activity. Protein extracts from *T. cruzi* epimastigotes were exposed to a fixed 28 μM concentration of each compound. The enzyme inhibition induced by Na mpo was considered as 1 and used to determine the relative change in inhibition caused by each complex. The standard deviations (SD) for each compound represent the results of two independent experiments. Three separate experiments were conducted, each with two technical replicates (n = 6). ANOVA analysis in relation to inhibition caused by the free Na mpo ligand: ** = $p<0.01$, *** = $p<0.001$.

3.2.6 Interaction with *Trypanosoma cruzi* NADH-fumarate reductase (*Tc*FR)

Mpo ligand has been described as an inhibitor of the NADH-dependent *T. cruzi* fumarate reductase (*Tc*FR) enzyme activity (Turrens et al., 1999). The background on mpo anti-*T.cruzi* activity together with the research previously performed by our group with classical and organometallic coordination compounds with mpo as a ligand (Vieites et al., 2008; Vieites et al., 2009; Rodriguez Arce et al., 2015), motivated postulating *Tc*FR as a potential target of the [V^{IV}O(L-H)(mpo)] compounds. Protein extracts of *T. cruzi* epimastigotes were treated with the sodium salt of mpo and with all [V^{IV}O(L-H)(mpo)] complexes. A statistically significant increase in the inhibitory effect of *Tc*FR

activity was observed for the complexes with respect to the ligand in its free form (Figure 8).

The effect was similar for all compounds except for [V^{IV}O(L4-H)(mpo)], which shows a higher inhibitory activity. This result correlates with the observed *in vitro* activity against *T. cruzi* (Table 2). [V^{IV}O(L4-H)(mpo)] shows the lowest IC$_{50, 24 h}$ of the series (IC$_{50, 24 h}$ epimastigotes: 0.83 μM; IC$_{50, 24 h}$ trypomastigotes: 0.19 μM). Although the trend is not clear for the rest of the series, since the relative inhibition values were similar and the IC$_{50, 24 h}$ shown in Table 2 do not have large differences, this finding suggests that the *Tc*FR enzyme could be a target for this series of compounds. At the working concentration, the compounds exhibit an inhibitory effect approximately 4-fold greater than the previously reported for

FIGURE 9
Structural features of the NADH-*Tc*FR: [V^{IV}O(L2-H)(mpo)] complex at the most populated cluster from molecular docking into the catalytic domain of the holoenzyme (cartoon representation, in blue). **(A)** The overall location is shared by all the [V^{IV}O(L-H)(mpo)] series with close-ups of their position relative to NADH or the side chains of interacting amino acids. V^{IV}O species, NADH cofactor, and residues are represented in sticks, colored by element; amino acids labeled in green are conserved in the interaction network across the series. **(B)** Residue and type of interaction at each of the [V^{IV}O(L-H)(mpo)] compounds for L = L0-L4 at the pose from the most populated cluster in each case.

[M(dppf)(mpo)](PF$_6$), where M=Pd or Pt (Rodriguez Arce et al., 2015).

Exploratory ligand-protein docking was conducted initially to understand the nature and relative strength of the interactions between the V^{IV}O compounds and the soluble NADH-*Tc*FR holoenzyme. The study used DFT/PCM structures of the five [V^{IV}O(LH)(mpo)] compounds and a 3D all-domain NADH-*Tc*FR template. This template was recently generated by some of us (Salazar et al., 2023) loading NADH onto a protein scaffold predicted *in silico* with AlphaFold2 from the sequence of 1.215 residues of *Tc*FR and conducting molecular dynamics (MD) simulations (see Supporting Material). It is important to recall that no experimental *Tc*FR holo/apoenzyme structures are currently available.

Figure 9A shows a structure representing the most populated cluster formed by docking the complex [V^{IV}O(L-H)(mpo)] into the catalytic domain of the enzyme, taking this case with L = L2 as an example, exposing the remaining structures for L = L0, L1, L3, and L4 in Supplementary Figure S3. All five V^{IV}O species bind to the enzyme in a crevice far from the fumarate entrance channel and the site for its catalytic conversion to succinate by NADH's nicotinamide and Arg761. When it comes to orientation, [V^{IV}O(L-H)(mpo)] complexes for L = L0 and L1 (Supplementary Figure S3) have mpo pointing inwards, proximal to NADH's purine moiety in the cofactor pocket. Conversely, mpo is oriented towards the solvent-accessible protein surface for L = L2 (Figure 9), L3, and L4 (Supplementary Figure S3), inverting positions with these bulkier 8-hydroxyquinoline derivatives. The V^{IV}=O core is stabilized by accepting O...H-N hydrogen bonding from the backbone amide of Thr687 (all the species) and Asn667 (just for [V^{IV}O(L4-H)(mpo)]). Moreover, 8-HQ/mpo are both further stabilized mainly through C-H/π proline-aromatic interactions (Zondlo, 2013) within a hydrophobic cage formed by a variable number of proline residues (three for [V^{IV}O(L2-H)(mpo)] and

[V^{IV}O(L3-H)(mpo)]); two for ([V^{IV}O(L0-H)(mpo)] and [V^{IV}O(L1-H)(mpo)]); one for ([V^{IV}O(L4-H)(mpo)]). Additionally, other residues reinforce compound stabilization depending on the nature of L (Figure 9B). Regarding binding affinity (see Supplementary Table S4), although some modulation is observed by changing 8-HQ substituents, these effects do not explain the observed relative activity. The best candidates for this inhibitory action on NADH-*Tc*FR from non-covalent interactions on a rigid protein would expected to be, at first sight, [V^{IV}O(L3-H)(mpo)] and [V^{IV}O(L2-H)(mpo)], both bearing more polarizable iodine substituents. The next step is to introduce flexibility into the whole complex system through MD simulations.

All the NADH-*Tc*FR: [V^{IV}O(L-H)(mpo)] ternary complexes remained stable along the 500 ns MD simulations (see RMSDs over protein backbone and cofactor atoms in Supplementary Figure S4), retaining, at first sight, the overall structural features as shown in Figure 10. A closer examination in comparison to the holoenzyme structure and dynamics reveals mutual adaptation is taking place in a way modulated by the nature of L after [V^{IV}O(L-H)(mpo)] harboring in the remote location at the catalytic domain of the *T. cruzi* enzyme, corresponding to a hinge region between two subdomains distinguished in the former. The positioning of NADH at its binding pocket is affected (found to be significantly shifted for V^{IV}O complexes carrying L = L1/L2/L3, as shown in the close-ups in Figure 10 and the orange panels in Supplementary Figure S4) resulting not only in changes into the active site architecture that can compromise the available space for the substrate insertion between NADH's nicotinamide moiety and Arg761 (for which the C4$_{NADH}$...N$^\eta_{Arg761}$ distance fluctuating around 11 Å in the free of substrate holoenzyme, increases to 13–17 Å after interaction with [V^{IV}O(L-H)(mpo)] for L = L1-L2-L3 and appears, in turn, to be significantly reduced to 5–6 Å for the L = L4 case) but propagating from the hinge region up to the
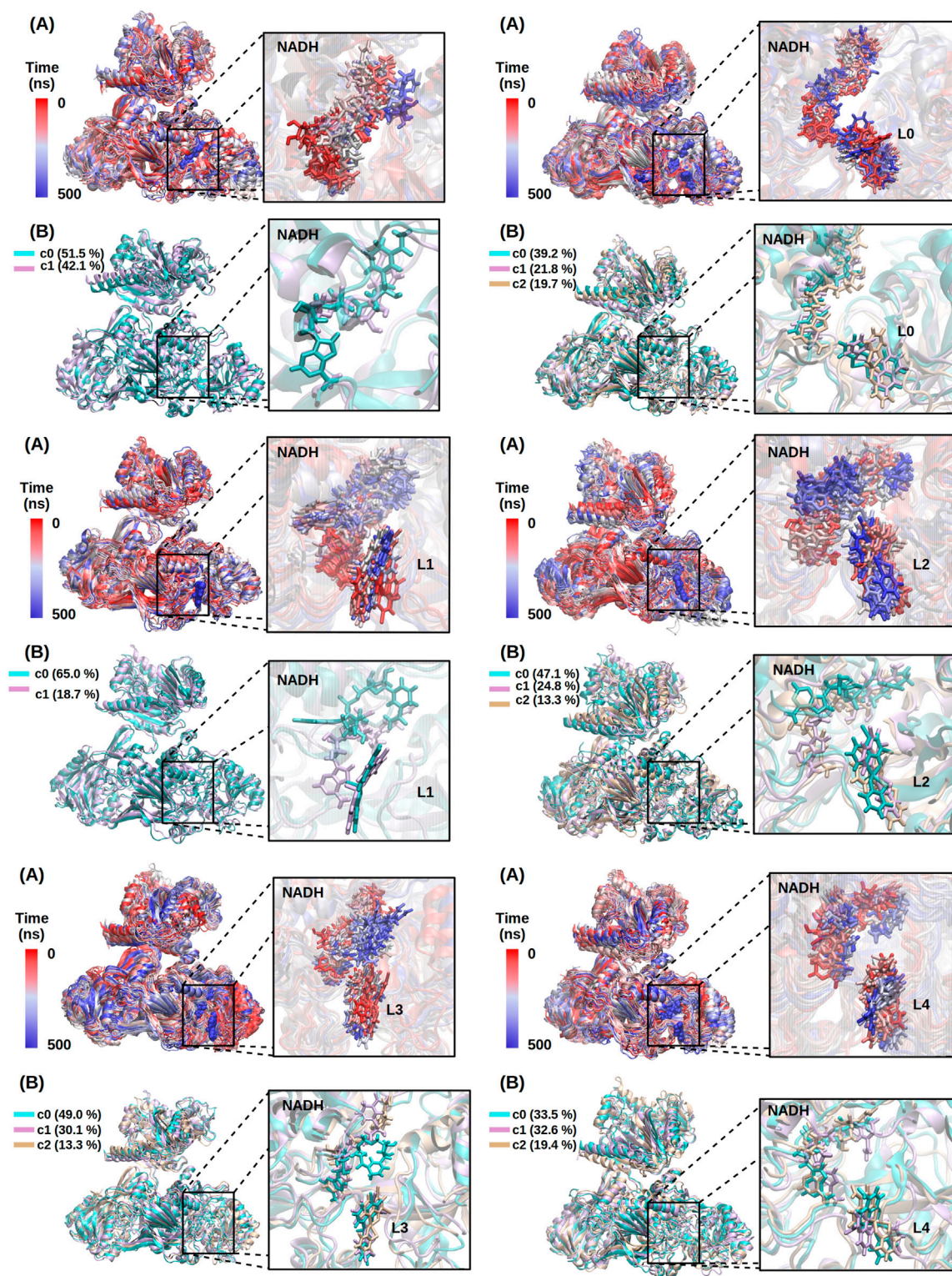
FIGURE 10
Structure and dynamics along the 500 ns MD simulation for NADH-TcFR (upper left) and NADH-TcFR:[V^{IV}O(L-H)(mpo)] ternary complexes with L = L0 (upper right), L1 and L2 (center left and right, respectively), L3 and L4 (bottom left and right, respectively). Panel **(A)** Time evolution of the structure going from red to blue. Panel **(B)** overlay of representative structures from principal clusters in each case, colored in cyan, magenta, and gold with an indication of their population percentage. Protein represented in the cartoon, cofactor, and ligands are shown in sticks in the corresponding close-up.

entrance of the substrate channel -monitored through the $C^{\alpha}_{Gly568}\cdots C^{\alpha}_{Val844}$ distance as shown in Supplementary Figure S5, that also fluctuates between open and close conformations-by affecting protein intradomain dynamics in the sub-microsecond time scale. Trends in MM-PB(GB)SA binding free-energies (collected in Supplementary Table S5) sustain [V^{IV}O(L3-H)(mpo)] as the compound with the highest affinity toward NADH-TcFR in the series, whereas after enabling TcFR and cofactor flexibility, mutual adjustments enhance the [V^{IV}O(L1-H)(mpo)] interaction network, upgrading to the second place in this ranking.

These findings, needing further experimental corroboration whenever possible, might be at the roots of the inhibitory activity reported in Figure 8, slightly modulated by the nature of the substituents in L and involving a distinct mode of action with respect to Na^{+}(mpo^{-}) and other M-mpo derived species previously examined by our group (Rodriguez Arce et al., 2015; Santos and Pessoa, 2023). The interaction in a distal binding site promotes a structural reorganization in the holoenzyme that starts affecting the cofactor positioning within its binding pocket and ultimately propagates up to the entrance channel, altering the dynamics of the opening/closure to the substrate in the sub-microseconds time scale and, for some [V^{IV}O(L-H)(mpo)] such as the one with L = L4, makes NADH unable to adopt the optimal arrangement required at the active site for reducing fumarate to succinate, globally resulting in partial abolition of the catalytic activity.

4 Conclusion

In summary, we successfully synthesized and characterized a novel series of five oxidovanadium(IV) heteroleptic compounds, denoted as [V^{IV}O(L-H)(mpo)], featuring 8-hydroxyquinoline derivatives (L) and 2-mercaptopyridine N-oxide (mpo). These compounds displayed notable activity against both epimastigote and trypomastigote life cycle forms of T. cruzi (CL Brener strain), as well as against promastigotes of L. infantum. Remarkably, the infective trypomastigote form of T. cruzi was more sensitive to the [V^{IV}O(L-H)(mpo)] compounds, with IC$_{50}$ values surpassing those of Nifurtimox. Regrettably, the compounds were more toxic and less selective towards the parasites than the free ligands. Among the synthesized complexes, [V^{IV}O(L2-H)(mpo)] emerged as a candidate for further investigation, as it demonstrated significant impacts on the infection process and the proliferation of intracellular amastigotes. Metallomics type analysis revealed preferential accumulation in the soluble proteins fraction, with only small amounts localized in the DNA fraction, discarding DNA as a primary target.

Biological assays unveiled a trypanocidal effect for all doses of [V^{IV}O(L2-H)(mpo)], with indications of apoptosis as the primary mode of cell death. The generation of reactive oxygen species (ROS) and compromised mitochondrial membrane potential in treated parasites suggest oxidative stress in parasites, while moderate dysregulation of mitochondrial membrane integrity hints at the induction of mitochondria-dependent apoptosis.

Exploratory ligand-protein docking followed by sub-microsecond molecular dynamics simulations for the V^{IV}O-compounds targeting soluble T. cruzi NADH-dependent fumarate reductase (NADH-TcFR) were consistent in finding all complexes of the series bind in a hinge region within the holoenzyme catalytic domain, distal to the active site and the putative fumarate entrance channel, preferred by Na^{+}(mpo^{-}) and other M-mpo-derived NADH-TcFR inhibitors previously addressed by us under similar or the same strategies (Machado et al., 2015; Rodriguez Arce et al., 2015; Salazar et al., 2023). Their relative affinity for TcFR appears to be modulated in some extension by the nature of the 8-HQ derivative, although not the only determinant of their inhibitory activity. Within the time scale explored, [V^{IV}O(L-H)(mpo)] binding would be inducing cofactor shifting/reorientation with impact on the architecture of the active site and affecting protein intradomain dynamics at the opening/closure of the substrate entrance channel, articulated from the hinge region. This paved the way for a first proposal to rationalize the inhibitory action confirmed through in vitro experiments using T. cruzi protein extracts. Collectively, our findings support the notion that the inhibition of this parasite-specific enzyme plays a role in the trypanocidal action of these complexes.

This last observation agrees with the belief that the binding of vanadium species to proteins and interference with their role in cells is a relevant step in the mechanism of action of vanadium complexes (or their hydrolysis products). The IC$_{50}$ values are in the low µM range. Thus, most probably the complexes will hydrolyze extensively, and the vanadium possibly binds to ligands present in the incubation medium in much higher concentration such as BSA, as was found in other similar systems (Nunes et al., 2020; Nunes et al., 2021). In this context, it is expected that the complexes dissociate, and the free metal ion and ligands exert their biological activity separately. Consequently, the complexes [V^{IV}O(L-H)(mpo)] are envisioned to function as pro-drugs. Many structural studies, namely, by single crystal X-ray diffraction, confirm the interaction of vanadium complexes with proteins, as well as the relevance of their partial hydrolysis (Santos and Pessoa, 2023). Namely, crystallographic and theoretical studies addressing the interaction of V^{IV}(8HQ)$_2$ with bovine pancreatic ribonuclease (RNase A) confirmed the partial hydrolysis of the V^{IV}(8HQ)$_2$ complex, and the binding of the V^{IV}O(8HQ)(H$_2$O)$^{+}$ adduct to the enzyme (Ferraro et al., 2023).

Mitochondrial deficiency as well as protein expression analysis with (VOSalophen), where Salophen is a Schiff base of a stilbene derivative (Machado et al., 2015), showed overexpression of transporters and drug efflux proteins as well as some proteins involved in transcription. This included overexpression of some proteins involved in hydrolysis and redox pathways, implying that the mentioned vanadium complex is responsible for some redox disorders. This study agrees with the results obtained in this work.

These promising results encourage further investigations and the development of prospective antitrypanosomal agents centered on vanadium-based compounds, particularly addressing their use as pro-drugs, namely, making modifications of [V^{IV}O(L-H)(mpo)] compounds to improve selectivity. This research holds great potential for advancing our understanding of trypanosomiasis treatment and drug development strategies.

Data availability statement

The original contributions presented in the study are included in the article/Supplementary Material, further inquiries can be directed to the corresponding authors.

Ethics statement

Ethical approval was not required for the studies performed because commercially available established cell lines were used.

Author contributions

GS: Conceptualization, Investigation, Visualization, Writing–original draft, Writing–review and editing, Data curation, Formal Analysis, Methodology. IM: Formal Analysis, Investigation, Methodology, Writing–review and editing. FS: Formal Analysis, Investigation, Methodology, Data curation, Visualization. ELC: Conceptualization, Data Curation, Methodology, Resources, Supervision, Validation, writing–original draft, writing–review and editing. IC: Formal Analysis, Funding acquisition, Investigation, Methodology, Writing–review and editing. JP: Conceptualization, Writing–review and editing. LP-D: Conceptualization, Data curation, Formal Analysis, Investigation, Methodology, Supervision, Visualization, Writing–review and editing. DG: Conceptualization, Funding acquisition,Methodology, Investigation, Project administration, Resources, Supervision, Validation, Visualization, Writing–original draft, Writing–review and editing.

Funding

Acknowledgments

Conflict of interest

The authors declare that the research was conducted in the absence of any commercial or financial relationships that could be construed as a potential conflict of interest.

The author(s) declared that they were an editorial board member of Frontiers, at the time of submission. This had no impact on the peer review process and the final decision.

Publisher's note

All claims expressed in this article are solely those of the authors and do not necessarily represent those of their affiliated organizations, or those of the publisher, the editors and the reviewers. Any product that may be evaluated in this article, or claim that may be made by its manufacturer, is not guaranteed or endorsed by the publisher.

Supplementary material

The Supplementary Material for this article can be found online at: https://www.frontiersin.org/articles/10.3389/fchbi.2023.1304571/full#supplementary-material

References

Ammerman, N. C., Beier-Sexton, M., and Azad, A. F. (2008). Growth and maintenance of Vero cell lines. *Curr. Protoc. Microbiol.* Appendix 4, Appendix 4E. doi:10.1002/9780471729259.mca04es11

Benitez, J., Becco, L., Correia, I., Leal, S. M., Guiset, H., Pessoa, J. C., et al. (2011). Vanadium polypyridyl compounds as potential antiparasitic and antitumoral agents: new achievements. *J. Inorg. Biochem.* 105 (2), 303–312. doi:10.1016/j.jinorgbio.2010.11.001

Benitez, J., Guggeri, L., Tomaz, I., Pessoa, J. C., Moreno, V., Lorenzo, J., et al. (2009). A novel vanadyl complex with a polypyridyl DNA intercalator as ligand: a potential anti-protozoa and anti-tumor agent. *J. Inorg. Biochem.* 103 (10), 1386–1394. doi:10.1016/j.jinorgbio.2009.07.013

Bondi, A. (1964). van der Waals volumes and radii. *J. Phys. Chem.* 68 (3), 441–451. doi:10.1021/j100785a001

Brindha, J., Balamurali, M., and Chanda, K. (2021). An overview on the therapeutics of neglected infectious diseases-Leishmaniasis and Chagas diseases. *Front. Chem.* 9, 1–19. doi:10.3389/fchem.2021.622286

Brown, R. W., and Hyland, C. J. T. (2015). Medicinal organometallic chemistry – an emerging strategy for the treatment of neglected tropical diseases. *Med. Chem. Comm.* 6 (7), 1230–1243. doi:10.1039/c5md00174a

Burza, S., Croft, S. L., and Boelaert, M. (2018). Leishmaniasis. *Lancet* 392 (10151), 951–970. doi:10.1016/s0140-6736(18)31204-2

Bustos, P. L., Volta, B. J., Perrone, A. E., Milduberger, N., and Bua, J. (2017). A homolog of cyclophilin D is expressed in Trypanosoma cruzi and is involved in the oxidative stress-damage response. *Cell Death Discov.* 3, 16092. doi:10.1038/cddiscovery.2016.92

Chai, J.-D., and Head-Gordon, M. (2008). Long-range corrected hybrid density functionals with damped atom–atom dispersion corrections. *Phys. Chem. Chem. Phys.* 10 (44), 6615–6620. doi:10.1039/b810189b

Chasteen, N. D. (1981). Vanadyl (IV) EPR spin probes inorganic and biochemical aspects. *Biol. Magn. Reson.* 3, 53–119. doi:10.1007/978-1-4613-3201-5_2

Christmas, P. B., and Turrens, J. F. (2000). Separation of NADH-fumarate reductase and succinate dehydrogenase activities in Trypanosoma cruzi. *FEMS Microbiol. Lett.* 183, 225–228. doi:10.1111/j.1574-6968.2000.tb08962.x

Cipriani, M., Toloza, J., Bradford, L., Putzu, E., Vieites, M., Curbelo, E., et al. (2014). Effect of the metal ion on the anti T. cruzi activity and mechanism of action of 5-nitrofuryl-containing thiosemicarbazone metal complexes. *Eur. J. Inorg. Chem.* 2014 (27), 4677–4689. doi:10.1002/ejic.201402614

Correia, I., Adao, P., Roy, S., Wahba, M., Matos, C., Maurya, M. R., et al. (2014). Hydroxyquinoline derived vanadium(IV and V) and copper(II) complexes as potential anti-tuberculosis and anti-tumor agents. *J. Inorg. Biochem.* 141, 83–93. doi:10.1016/j.jinorgbio.2014.07.019

Costa Pessoa, J., Garribba, E., Santos, M. F. A., and Santos-Silva, T. (2015). Vanadium and proteins: uptake, transport, structure, activity and function. *Coord. Chem. Rev.* 301-302, 49–86. doi:10.1016/j.ccr.2015.03.016

Deolindo, P., Teixeira-Ferreira, A. S., Melo, E. J., Arnholdt, A. C. V., Souza, W. D., Alves, E. W., et al. (2005). Programmed cell death in Trypanosoma cruzi induced by *Bothrops jararaca* venom. *Memorias do Inst. Oswaldo Cruz* 100 (1), 33–38. doi:10.1590/s0074-02762005000100006

De Rycker, M., Baragana, B., Duce, S. L., and Gilbert, I. H. (2018). Challenges and recent progress in drug discovery for tropical diseases. *Nature* 559 (7715), 498–506. doi:10.1038/s41586-018-0327-4

Ditchfield, R., Hehre, W. J., and Pople, J. A. (1971). Self-consistent molecular-orbital methods. IX. An extended Gaussian-type basis for molecular-orbital studies of organic molecules. *J. Chem. Phys.* 54 (2), 724–728. doi:10.1063/1.1674902

Docampo, R. (1990). Sensitivity of parasites to free radical damage by antiparasitic drugs. *Chemico-biological Interact.* 73 (1), 1–27. doi:10.1016/0009-2797(90)90106-w

Docampo, R., and Vercesi, A. E. (2022). Mitochondrial Ca^{2+} and reactive oxygen species in trypanosomatids. *Antioxidants Redox Signal.* 36, 969–983. doi:10.1089/ars.2021.0058

Fernandez, M., Becco, L., Correia, I., Benitez, J., Piro, O. E., Echeverria, G. A., et al. (2013a). Oxidovanadium(IV) and dioxidovanadium(V) complexes of tridentate salicylaldehyde semicarbazones: searching for prospective antitrypanosomal agents. *J. Inorg. Biochem.* 127, 150–160. doi:10.1016/j.jinorgbio.2013.02.010

Fernandez, M., Varela, J., Correia, I., Birriel, E., Castiglioni, J., Moreno, V., et al. (2013b). A new series of heteroleptic oxidovanadium(IV) compounds with phenanthroline-derived co-ligands: selective Trypanosoma cruzi growth inhibitors. *Dalton Trans.* 42 (33), 11900–11911. doi:10.1039/c3dt50512j

Ferraro, G., Vitale, L., Sciortino, G., Pisanu, F., Garribba, E., and Merlino, A. (2023). Interaction of V IV O–8-hydroxyquinoline species with RNase A: the effect of metal ligands in the protein adduct stabilization. *Inorg. Chem. Front.* 10 (17), 5186–5198. doi:10.1039/d3qi01023f

Floris, F., and Tomasi, J. (1989). Evaluation of the dispersion contribution to the solvation energy. A simple computational model in the continuum approximation. *J. Comput. Chem.* 10 (5), 616–627. doi:10.1002/jcc.540100504

Floris, F., Tomasi, J., and Ahuir, J. L. P. (1991). Dispersion and repulsion contributions to the solvation energy: refinements to a simple computational model in the continuum approximation. *J. Comput. Chem.* 12 (7), 784–791. doi:10.1002/jcc.540120703

Francl, M. M., Pietro, W. J., Hehre, W. J., Binkley, J. S., Gordon, M. S., DeFrees, D. J., et al. (1982). Self-consistent molecular orbital methods. XXIII. A polarization-type basis set for second-row elements. *J. Chem. Phys.* 77 (7), 3654–3665. doi:10.1063/1.444267

Frisch, M. J., Trucks, G. W., Schlegel, H. B., Scuseria, G. E., Robb, M. A., Cheeseman, J. R., et al. (2019). *Gaussian 16, revision C. 01*. Wallingford CT: Gaussian, Inc.

Fuhrmann, J., Rurainski, A., Lenhof, H. P., and Neumann, D. (2010). A new Lamarckian genetic algorithm for flexible ligand-receptor docking. *J. Comput. Chem.* 31 (9), 1911–1918. doi:10.1002/jcc.21478

Gambino, D. (2011). Potentiality of vanadium compounds as anti-parasitic agents. *Coord. Chem. Rev.* 255 (19-20), 2193–2203. doi:10.1016/j.ccr.2010.12.028

Gambino, D., and Otero, L. (2012). Perspectives on what ruthenium-based compounds could offer in the development of potential antiparasitic drugs. *Inorganica Chim. Acta* 393, 103–114. doi:10.1016/j.ica.2012.05.028

Gambino, D., and Otero, L. (2018). Design of prospective antiparasitic metal-based compounds including selected organometallic cores. *Inorganica Chim. Acta* 472, 58–75. doi:10.1016/j.ica.2017.07.068

Gambino, D., and Otero, L. (2019). "Metal compounds in the development of antiparasitic agents; rational design from basic chemistry to the clinic," in *Essential metals in medicine: therapeutic use and toxicity of metal ions in the clinic*. Editor P. Carver (Berlin, Germany: Walter de Gruyter), 331–358.

Gambino, D., and Otero, L. (2021). Facing diseases caused by trypanosomatid parasites: rational design of Pd and Pt complexes with bioactive ligands. *Front. Chem.* 9, 816266. doi:10.3389/fchem.2021.816266

Gambino, D., and Otero, L. (2023). "Prospective metallo-drugs including bioactive compounds: selection of co-ligands to tune biological activity against neglected tropical diseases," in *Targeted metallo-drugs: design, development, and modes of action*. Editors M. Etelka and C. J. Marmion (Boca Raton, United States: CRC Press), 193.

Gasteiger, J., and Marsili, M. (1978). A new model for calculating atomic charges in molecules. *Tetrahedron Lett.* 19 (34), 3181–3184. doi:10.1016/s0040-4039(01)94977-9

Gasteiger, J., and Marsili, M. (1980). Iterative partial equalization of orbital electronegativity—a rapid access to atomic charges. *Tetrahedron* 36 (22), 3219–3228. doi:10.1016/0040-4020(80)80168-2

Genes, C., Baquero, E., Echeverri, F., Maya, J. D., and Triana, O. (2011). Mitochondrial dysfunction in Trypanosoma cruzi: the role of *Serratia marcescens* prodigiosin in the alternative treatment of Chagas disease. *Parasites vectors* 4 (1), 66–68. doi:10.1186/1756-3305-4-66

Gibson, D. (2019). Multi-action Pt (IV) anticancer agents; do we understand how they work? *J. Inorg. Biochem.* 191, 77–84. doi:10.1016/j.jinorgbio.2018.11.008

Gupta, R., Luxami, V., and Paul, K. (2021). Insights of 8-hydroxyquinolines: a novel target in medicinal chemistry. *Bioorg. Chem.* 108, 104633. doi:10.1016/j.bioorg.2021.104633

Hariharan, P. C., and Pople, J. A. (1973). The influence of polarization functions on molecular orbital hydrogenation energies. *Theor. Chim. acta* 28, 213–222. doi:10.1007/bf00533485

Hay, P. J., and Wadt, W. R. (1985a). *Ab initio* effective core potentials for molecular calculations. Potentials for the transition metal atoms Sc to Hg. *J. Chem. Phys.* 82 (1), 270–283. doi:10.1063/1.448799

Hay, P. J., and Wadt, W. R. (1985b). *Ab initio* effective core potentials for molecular calculations. Potentials for K to Au including the outermost core orbitals. *J. Chem. Phys.* 82 (1), 299–310. doi:10.1063/1.448975

Irigoin, F., Inada, N. M., Fernandes, M. P., Piacenza, L., Gadelha, F. R., Vercesi, A. E., et al. (2009). Mitochondrial calcium overload triggers complement-dependent superoxide-mediated programmed cell death in Trypanosoma cruzi. *Biochem. J.* 418 (3), 595–604. doi:10.1042/bj20081981

Joaquim, A. R., Gionbelli, M. P., Gosmann, G., Fuentefria, A. M., Lopes, M. S., and Fernandes de Andrade, S. (2021). Novel antimicrobial 8-hydroxyquinoline-based agents: current development, structure–activity relationships, and perspectives. *J. Med. Chem.* 64 (22), 16349–16379. doi:10.1021/acs.jmedchem.1c01318

Katsuno, K., Burrows, J. N., Duncan, K., Van Huijsduijnen, R. H., Kaneko, T., Kita, K., et al. (2015). Hit and lead criteria in drug discovery for infectious diseases of the developing world. *Nat. Rev. drug Discov.* 14 (11), 751–758. doi:10.1038/nrd4683

Kenny, R. G., and Marmion, C. J. (2019). Toward multi-targeted platinum and ruthenium drugs—a new paradigm in cancer drug treatment regimens? *Chem. Rev.* 119 (2), 1058–1137. doi:10.1021/acs.chemrev.8b00271

Kessler, R. L., Soares, M. J., Probst, C. M., and Krieger, M. A. (2013). Trypanosoma cruzi response to sterol biosynthesis inhibitors: morphophysiological alterations leading to cell death. *PLoS One* 8 (1), e55497. doi:10.1371/journal.pone.0055497

Kourbeli, V., Chontzopoulou, E., Moschovou, K., Pavlos, D., Mavromoustakos, T., and Papanastasiou, I. P. (2021). An overview on target-based drug design against kinetoplastid Protozoan infections: human african trypanosomiasis, Chagas disease and leishmaniases. *Molecules* 26 (15), 4629. doi:10.3390/molecules26154629

Kowalski, S., Wyrzykowski, D., and Inkielewicz-Stępniak, I. (2020). Molecular and cellular mechanisms of cytotoxic activity of vanadium compounds against cancer cells. *Molecules* 25 (7), 1757. doi:10.3390/molecules25071757

Kroemer, G. (1997). Mitochondrial implication in apoptosis. Towards an endosymbiont hypothesis of apoptosis evolution. *Cell Death Differ.* 4 (6), 443–456. doi:10.1038/sj.cdd.4400266

Kwofie, S. K., Broni, E., Dankwa, B., Enninful, K. S., Kwarko, G. B., Darko, L., et al. (2020). Outwitting an old neglected nemesis: a review on leveraging integrated data-driven approaches to aid in unraveling of leishmanicides of therapeutic potential. *Curr. Top. Med. Chem.* 20 (5), 349–366. doi:10.2174/1568026620666200128160454

Levina, A., Crans, D. C., and Lay, P. A. (2017). Speciation of metal drugs, supplements and toxins in media and bodily fluids controls *in vitro* activities. *Coord. Chem. Rev.* 352, 473–498. doi:10.1016/j.ccr.2017.01.002

Levina, A., and Lay, P. A. (2017). Stabilities and biological activities of vanadium drugs: what is the nature of the active species? *Chem. - Asian J.* 12 (14), 1692–1699. doi:10.1002/asia.201700463

Machado, I., Marino, L. B., Demoro, B., Echeverría, G. A., Piro, O. E., Leite, C. Q., et al. (2014). Bioactivity of pyridine-2-thiolato-1-oxide metal complexes: Bi (III), Fe (III) and Ga (III) complexes as potent anti-Mycobacterium tuberculosis prospective agents. *Eur. J. Med. Chem.* 87, 267–273. doi:10.1016/j.ejmech.2014.09.067

Machado, P. d. A., Mota, V. Z., Cavalli, A. C. d. L., de Carvalho, G. S. G., Da Silva, A. D., Gameiro, J., et al. (2015). High selective antileishmanial activity of vanadium complex with stilbene derivative. *Acta trop.* 148, 120–127. doi:10.1016/j.actatropica.2015.04.018

MacLean, L. M., Thomas, J., Lewis, M. D., Cotillo, I., Gray, D. W., and De Rycker, M. (2018). Development of Trypanosoma cruzi *in vitro* assays to identify compounds suitable for progression in Chagas' disease drug discovery. *PLoS Neglected Trop. Dis.* 12 (7), e0006612. doi:10.1371/journal.pntd.0006612

Menna-Barreto, R. F. S. (2019). Cell death pathways in pathogenic trypanosomatids: lessons of (over)kill. *Cell Death Dis.* 10 (2), 93–11. doi:10.1038/s41419-019-1370-2

Micera, G., Pecoraro, V. L., and Garribba, E. (2009). Assessing the dependence of ^{51}V a_z value on the aromatic ring orientation of $V^{IV}O^{2+}$ pyridine complexes. *Inorg. Chem.* 48 (13), 5790–5796. doi:10.1021/ic9001779

Minori, K., Rosa, L. B., Bonsignore, R., Casini, A., and Miguel, D. C. (2020). Comparing the antileishmanial activity of gold (I) and gold (III) compounds in L. Amazonensis and L. Braziliensis *in vitro*. *ChemMedChem* 15 (22), 2146–2150. doi:10.1002/cmdc.202000536

Morris, G. M., Goodsell, D. S., Halliday, R. S., Huey, R., Hart, W. E., Belew, R. K., et al. (1998). Automated docking using a Lamarckian genetic algorithm and an empirical binding free energy function. *J. Comput. Chem.* 19 (14), 1639–1662. doi:10.1002/(sici)1096-987x(19981115)19:14<1639::aid-jcc10>3.0.co;2-b

Morris, G. M., Huey, R., Lindstrom, W., Sanner, M. F., Belew, R. K., Goodsell, D. S., et al. (2009). AutoDock4 and AutoDockTools4: automated docking with selective receptor flexibility. *J. Comput. Chem.* 30 (16), 2785–2791. doi:10.1002/jcc.21256

Mosquillo, M. F., Bilbao, L., Hernandez, F., Machado, I., Gambino, D., Garat, B., et al. (2018a). Effect of a new anti-T. cruzi metallic compound based on palladium. *Biometals* 31 (6), 961–974. doi:10.1007/s10534-018-0140-4

Mosquillo, M. F., Bilbao, L., Hernandez, F., Tissot, F., Gambino, D., Garat, B., et al. (2018b). Trypanosoma cruzi biochemical changes and cell death induced by an organometallic platinum-based compound. *Chem. Biol. Drug Des.* 92 (3), 1657–1669. doi:10.1111/cbdd.13332

Mosquillo, M. F., Smircich, P., Ciganda, M., Lima, A., Gambino, D., Garat, B., et al. (2020a). Comparative high-throughput analysis of the Trypanosoma cruzi response to organometallic compounds. *Metallomics* 12 (5), 813–828. doi:10.1039/d0mt00030b

Mosquillo, M. F., Smircich, P., Lima, A., Gehrke, S. A., Scalese, G., Machado, I., et al. (2020b). High throughput approaches to unravel the mechanism of action of a new vanadium-based compound against trypanosoma cruzi. *Bioinorganic Chem. Appl.* 2020, 1–10. doi:10.1155/2020/1634270

Nagle, A. S., Khare, S., Kumar, A. B., Supek, F., Buchynskyy, A., Mathison, C. J., et al. (2014). Recent developments in drug discovery for leishmaniasis and human African trypanosomiasis. *Chem. Rev.* 114 (22), 11305–11347. doi:10.1021/cr500365f

Navarro, M. (2009). Gold complexes as potential anti-parasitic agents. *Coord. Chem. Rev.* 253 (11-12), 1619–1626. doi:10.1016/j.ccr.2008.12.003

Navarro, M., Gabbiani, C., Messori, L., and Gambino, D. (2010). Metal-based drugs for malaria, trypanosomiasis and leishmaniasis: recent achievements and perspectives. *Drug Discov. Today* 15 (23-24), 1070–1078. doi:10.1016/j.drudis.2010.10.005

Navarro, M., Justo, R., Delgado, G. Y. S., and Visbal, G. (2021). Metallodrugs for the treatment of trypanosomatid diseases: recent advances and new insights. *Curr. Pharm. Des.* 27 (15), 1763–1789. doi:10.2174/1381612826666201113104633

Nunes, P., Correia, I., Cavaco, I., Marques, F., Pinheiro, T., Avecilla, F., et al. (2021). Therapeutic potential of vanadium complexes with 1, 10-phenanthroline ligands, *quo vadis*? Fate of complexes in cell media and cancer cells. *J. Inorg. Biochem.* 217, 111350. doi:10.1016/j.jinorgbio.2020.111350

Nunes, P., Correia, I., Marques, F., Matos, A. P., Dos Santos, M. M., Azevedo, C. G., et al. (2020). Copper complexes with 1, 10-phenanthroline derivatives: underlying factors affecting their cytotoxicity. *Inorg. Chem.* 59 (13), 9116–9134. doi:10.1021/acs.inorgchem.0c00925

Oliveri, V., and Vecchio, G. (2016). 8-Hydroxyquinolines in medicinal chemistry: a structural perspective. *Eur. J. Med. Chem.* 120, 252–274. doi:10.1016/j.ejmech.2016.05.007

Ong, Y. C., Roy, S., Andrews, P. C., and Gasser, G. (2019). Metal compounds against neglected tropical diseases. *Chem. Rev.* 119 (2), 730–796. doi:10.1021/acs.chemrev.8b00338

Pessoa, J. C., and Correia, I. (2021). Misinterpretations in evaluating interactions of vanadium complexes with proteins and other biological targets. *Inorganics* 9 (2), 17. doi:10.3390/inorganics9020017

Pessoa, J. C., Etcheverry, S., and Gambino, D. (2015). Vanadium compounds in medicine. *Coord. Chem. Rev.* 301-302, 24–48. doi:10.1016/j.ccr.2014.12.002

Pessoa, J. C., Santos, M. F., Correia, I., Sanna, D., Sciortino, G., and Garribba, E. (2021). Binding of vanadium ions and complexes to proteins and enzymes in aqueous solution. *Coord. Chem. Rev.* 449, 214192. doi:10.1016/j.ccr.2021.214192

Pierotti, R. A. (1976). A scaled particle theory of aqueous and nonaqueous solutions. *Chem. Rev.* 76 (6), 717–726. doi:10.1021/cr60304a002

Rassolov, V. A., Pople, J. A., Ratner, M. A., and Windus, T. L. (1998). 6-31G* basis set for atoms K through Zn. *J. Chem. Phys.* 109 (4), 1223–1229. doi:10.1063/1.476673

Rivas, F., Del Mármol, C., Scalese, G., Pérez-Díaz, L., Machado, I., Blacque, O., et al. (2022). New multifunctional Ru(II) organometallic compounds show activity against Trypanosoma brucei and Leishmania infantum. *J. Inorg. Biochem.* 237, 112016. doi:10.1016/j.jinorgbio.2022.112016

Rivas, F., Medeiros, A., Quiroga, C., Benitez, D., Comini, M., Rodriguez-Arce, E., et al. (2021). New Pd-Fe ferrocenyl antiparasitic compounds with bioactive 8-hydroxyquinoline ligands: a comparative study with their Pt-Fe analogues. *Dalton Trans.* 50 (5), 1651–1665. doi:10.1039/d0dt03963b

Rockenbauer, A., and Korecz, L. (1996). Automatic computer simulations of ESR spectra. *Appl. Magn. Reson.* 10, 29–43. doi:10.1007/bf03163097

Rodriguez Arce, E., Mosquillo, M. F., Perez-Diaz, L., Echeverria, G. A., Piro, O. E., Merlino, A., et al. (2015). Aromatic amine N-oxide organometallic compounds: searching for prospective agents against infectious diseases. *Dalton Trans.* 44 (32), 14453–14464. doi:10.1039/c5dt00557d

Rodríguez Arce, E., Sarniguet, C., Moraes, T. S., Vieites, M., Tomaz, A. I., Medeiros, A., et al. (2015). A new ruthenium cyclopentadienyl azole compound with activity on tumor cell lines and trypanosomatid parasites. *J. Coord. Chem.* 68 (16), 2923–2937. doi:10.1080/00958972.2015.1062480

Salazar, F., Gambino, D., and Coitiño, E. L. (2023). Combining AlphaFold2 and molecular dynamics simulations to propose a new 3D structure for T.cruzi NADH-fumarate reductase: development and validation for *in silico* screening of transition metal-based selective antichagasic species. In preparation. *Target J. J. Comput. Chem.*

Sánchez-Delgado, R. A., and Anzellotti, A. (2004). Metal complexes as chemotherapeutic agents against tropical diseases: trypanosomiasis, malaria and leishmaniasis. *Mini Rev. Med. Chem.* 4 (1), 23–30. doi:10.2174/1389557043487493

Sánchez-Delgado, RAAA, and Suárez, L. (2004). "Metal ions and their complexes in medication," in *Metal ions in biological systems*. Editor H. S. A. Sigel (New York: Marcel Dekker), 379.

Sandes, J. M., Fontes, A., Regis-da-Silva, C. G., de Castro, M. C., Lima-Junior, C. G., Silva, F. P., et al. (2014). Trypanosoma cruzi cell death induced by the Morita-Baylis-Hillman adduct 3-Hydroxy-2-methylene-3-(4-nitrophenylpropanenitrile). *PLoS One* 9 (4), e93936. doi:10.1371/journal.pone.0093936

Sanna, D., Ugone, V., Micera, G., and Garribba, E. (2012). Temperature and solvent structure dependence of VO 2+ complexes of pyridine-N-oxide derivatives and their interaction with human serum transferrin. *Dalton Trans.* 41 (24), 7304–7318. doi:10.1039/c2dt12503j

Santoro, A., Calvo, J. S., Peris-Díaz, M. D., Krężel, A., Meloni, G., and Faller, P. (2020). The glutathione/metallothionein system challenges the design of efficient O2-activating copper complexes. *Angew. Chem. Int. Ed.* 59 (20), 7830–7835. doi:10.1002/anie.201916316

Santos, M. F., and Pessoa, J. C. (2023). Interaction of vanadium complexes with proteins: revisiting the reported structures in the protein data bank (PDB) since 2015. *Molecules* 28 (18), 6538. doi:10.3390/molecules28186538

Santos, M. F., Sciortino, G., Correia, I., Fernandes, A. C., Santos-Silva, T., Pisanu, F., et al. (2022). Binding of $V^{IV}O^{2+}$, $V^{IV}OL$, $V^{IV}OL_2$ and V^VO_2L moieties to proteins: X-ray/Theoretical characterization and biological implications. *Chem. (Weinheim der Bergstrasse, Ger.* 28 (40), e202200105. doi:10.1002/chem.202200105

Santos, S. S., de Araujo, R. V., Giarolla, J., Seoud, O. E., and Ferreira, E. I. (2020). Searching for drugs for Chagas disease, leishmaniasis and schistosomiasis: a review. *Int. J. Antimicrob. Agents* 55 (4), 105906. doi:10.1016/j.ijantimicag.2020.105906

Scalese, G., Benitez, J., Rostan, S., Correia, I., Bradford, L., Vieites, M., et al. (2015). Expanding the family of heteroleptic oxidovanadium(IV) compounds with salicylaldehyde semicarbazones and polypyridyl ligands showing anti-Trypanosoma cruzi activity. *J. Inorg. Biochem.* 147, 116–125. doi:10.1016/j.jinorgbio.2015.03.002

Scalese, G., Correia, I., Benitez, J., Rostan, S., Marques, F., Mendes, F., et al. (2017a). Evaluation of cellular uptake, cytotoxicity and cellular ultrastructural effects of heteroleptic oxidovanadium(IV) complexes of salicylaldimines and polypyridyl ligands. *J. Inorg. Biochem.* 166, 162–172. doi:10.1016/j.jinorgbio.2016.11.010

Scalese, G., Kostenkova, K., Crans, D. C., and Gambino, D. (2022). Metallomics and other omics approaches in antiparasitic metal-based drug research. *Curr. Opin. Chem. Biol.* 67, 102127. doi:10.1016/j.cbpa.2022.102127

Scalese, G., Machado, I., Correia, I., Pessoa, J. C., Bilbao, L., Pérez-Diaz, L., et al. (2019). Exploring oxidovanadium(iv) homoleptic complexes with 8-hydroxyquinoline derivatives as prospective antitrypanosomal agents. *New J. Chem.* 43 (45), 17756–17773. doi:10.1039/c9nj02589h

Scalese, G., Machado, I., Fontana, C., Risi, G., Salinas, G., Perez-Diaz, L., et al. (2018). New heteroleptic oxidovanadium(V) complexes: synthesis, characterization and biological evaluation as potential agents against *Trypanosoma cruzi*. *JBIC J. Biol. Inorg. Chem.* 23 (8), 1265–1281. doi:10.1007/s00775-018-1613-1

Scalese, G., Machado, I., Salinas, G., Perez-Diaz, L., and Gambino, D. (2021). Heteroleptic oxidovanadium(V) complexes with activity against infective and non-infective stages of *Trypanosoma cruzi*. *Molecules* 26 (17), 5375. doi:10.3390/molecules26175375

Scalese, G., Mosquillo, M. F., Rostan, S., Castiglioni, J., Alho, I., Perez, L., et al. (2017b). Heteroleptic oxidovanadium(IV) complexes of 2-hydroxynaphtyaldimine and polypyridyl ligands against Trypanosoma cruzi and prostate cancer cells. *J. Inorg. Biochem.* 175, 154–166. doi:10.1016/j.jinorgbio.2017.07.014

Smith, T. S., II, LoBrutto, R., and Pecoraro, VLJC. (2002). Paramagnetic spectroscopy of vanadyl complexes and its applications to biological systems. *Coord. Chem. Rev.* 228 (1), 1–18. doi:10.1016/s0010-8545(01)00437-4

Soba, M., Scalese, G., Casuriaga, F., Perez, N., Veiga, N., Echeverria, G. A., et al. (2023). Multifunctional organometallic compounds for the treatment of Chagas disease: Re(I) tricarbonyl compounds with two different bioactive ligands. *Dalton Trans.* 52 (6), 1623–1641. doi:10.1039/d2dt03869b

Song, Y., Xu, H., Chen, W., Zhan, P., and Liu, X. (2015). 8-Hydroxyquinoline: a privileged structure with a broad-ranging pharmacological potential. *Med. Chem. Comm.* 6 (1), 61–74. doi:10.1039/c4md00284a

Tahghighi, A. (2014). Importance of metal complexes for development of potential leishmanicidal agents. *J. Organomet. Chem.* 770, 51–60. doi:10.1016/j.jorganchem.2014.08.007

Tobin, D., Arvanitidis, M., and Bisby, R. H. (2002). One-electron oxidation of "photo-Fenton" reagents and inhibition of lipid peroxidation. *Biochem. biophysical Res. Commun.* 299 (1), 155–159. doi:10.1016/s0006-291x(02)02594-9

Tomasi, J., Mennucci, B., and Cancès, E. (1999). The IEF version of the PCM solvation method: an overview of a new method addressed to study molecular solutes at the QM *ab initio* level. *J. Mol. Struct. THEOCHEM* 464 (1-3), 211–226. doi:10.1016/s0166-1280(98)00553-3

Turrens, J. F., Newton, C. L., Zhong, L., Hernandez, F., Whitfield, J., and Docampo, R. (1999). Mercaptopyridine-N-oxide, an NADH-fumarate reductase inhibitor, blocks Trypanosoma cruzi growth in culture and in infected myoblasts. *FEMS Microbiol. Lett.* 175, 217–221. doi:10.1111/j.1574-6968.1999.tb13623.x

Veiga-Santos, P., Reignault, L. C., Huber, K., Bracher, F., De Souza, W., and De Carvalho, T. M. (2014). Inhibition of NAD+-dependent histone deacetylases (sirtuins) causes growth arrest and activates both apoptosis and autophagy in the pathogenic protozoan Trypanosoma cruzi. *Parasitology* 141 (6), 814–825. doi:10.1017/s0031182013001704

Viegas-Junior, C., Danuello, A., da Silva Bolzani, V., Barreiro, E. J., and Fraga, C. A. M. (2007). Molecular hybridization: a useful tool in the design of new drug prototypes. *Curr. Med. Chem.* 14 (17), 1829–1852. doi:10.2174/092986707781058805

Vieites, M., Smircich, P., Guggeri, L., Marchan, E., Gomez-Barrio, A., Navarro, M., et al. (2009). Synthesis and characterization of a pyridine-2-thiol N-oxide gold(I) complex with potent antiproliferative effect against Trypanosoma cruzi and Leishmania sp. insight into its mechanism of action. *J. Inorg. Biochem.* 103 (10), 1300–1306. doi:10.1016/j.jinorgbio.2009.02.011

Vieites, M., Smircich, P., Parajon-Costa, B., Rodriguez, J., Galaz, V., Olea-Azar, C., et al. (2008). Potent *in vitro* anti-Trypanosoma cruzi activity of pyridine-2-thiol N-oxide metal complexes having an inhibitory effect on parasite-specific fumarate reductase. *JBIC J. Biol. Inorg. Chem.* 13 (5), 723–735. doi:10.1007/s00775-008-0358-7

Williams, R. A., Smith, T. K., Cull, B., Mottram, J. C., and Coombs, G. H. (2012). ATG5 is essential for ATG8-dependent autophagy and mitochondrial homeostasis in Leishmania major. *PLoS Pathog.* 8 (5), e1002695. doi:10.1371/journal.ppat.1002695

World Health Organization (2023a). Chagas disease (also known as American trypanosomiasis). Available at: https://www.who.int/health-topics/chagas-disease#tab=tab_1 (accesed August, 2023).

World Health Organization (2023b). Leishmaniasis. Available at: https://www.who.int/news-room/fact-sheets/detail/leishmaniasis (accesed August, 2023).

World Health Organization (2023c). Neglected tropical diseases. Available at: https://www.who.int/news-room/q-a-detail/neglected-tropical-diseases (accesed August, 2023).

Wu, J. X., Hong, Y. H., and Yang, X. G. (2016). Bis(acetylacetonato)-oxidovanadium(IV) and sodium metavanadate inhibit cell proliferation via ROS-induced sustained MAPK/ERK activation but with elevated AKT activity in human pancreatic cancer AsPC-1 cells. *JBIC J. Biol. Inorg. Chem.* 21 (8), 919–929. doi:10.1007/s00775-016-1389-0

Wüthrich, K. (1965). Elektronenspinresonanz-Untersuchungen von VO2+-Komplexverbindungen in wässeriger Lösung II. *Helvetica Chim. Acta* 48 (5), 1012–1017. doi:10.1002/hlca.19650480504

Zamzami, N., Hirsch, T., Dallaporta, B., Petit, P. X., and Kroemer, G. (1997). Mitochondrial implication in accidental and programmed cell death: apoptosis and necrosis. *J. Bioenergetics Biomembr.* 29 (2), 185–193. doi:10.1023/a:1022694131572

Zhang, C., Bourgeade Delmas, S., Fernández Álvarez, Á., Valentin, A., Hemmert, C., and Gornitzka, H. (2018). Synthesis, characterization, and antileishmanial activity of neutral N-heterocyclic carbene gold (I) complexes. *Eur. J. Med. Chem.* 143, 1635–1643. doi:10.1016/j.ejmech.2017.10.060

Zondlo, N. (2013). Aromatic–proline interactions: electronically tunable CH/π interactions. *Accounts of Chemical Research* 46 (4), 1039–1049.